Polar ice-cores unravel the formation of a UV window during magnetic field collapse ~ 42 ka BP

Sanjeev Dasari[1*], Guillaume Paris[2], Julien Charreau[2], Alexis Lamothe[3†], Joel Savarino[3*]

[1]Deaprtment of Earth Sciences, University of Oxford, Oxford, United Kingdom

[2]Université de Lorraine, CNRS, CRPG, Nancy, France

[3]Institut des Géosciences de l'Environnement, University Grenoble Alpes, CNRS, IRD, Grenoble INP, Grenoble, France

[†]*Now at* International Center for Isotope Effects Research, Nanjing University, Nanjing, China

[*]*Corresponding author*: Sanjeev Dasari (sanjeev.dasari@earth.ox.ac.uk)

Joel Savarino (joel.savarino@cnrs.fr)

Key Points

- Observational evidence of strong ozone layer depletion in the Southern Hemisphere during the Laschamp Geomagnetic Excursion
- Timing of UV window formation is constrained to within 100 years of magnetic field collapse using sulfur isotope anomalies detected in ice core sulfate
- Potential for hemispherical discrepancy exists in the realization of the immediate effect of increased UV influx at Earth's surface during geomagnetic excursions

Abstract

During geomagnetic excursions (GEs), compromised magnetic field and increased cosmic-ray bombardment can deplete the ozone layer forming 'UV window(s)' in the Earth's atmosphere. Here, using triple sulfur-isotope systematics in polar ice-core sulfate record spanning 600 years of the Laschamp GE, we provide direct evidence of the formation of a UV window. Several events of UV-induced anomalous ice-core sulfate were detected under background conditions in Antarctica concomitant with the evolution of paleomagnetic intensity, with a distinct peak observed between ≈ 41.7 ka BP and ≈ 41.6 ka BP corresponding to the weakest magnetic field phase. The timing and amplitude of these events unequivocally confirm the existence of a UV window in the southern hemisphere during the LGE. However, such geochemical imprints were not detected in discrete sub-sampled northern polar ice-core record. We postulate that, among other possibilities, non-uniformity in excursion behaviour at the Earth's surface could be modulating this geochemical imprint.

Plain Language Summary

The ozone layer in the upper atmosphere acts as a shield against harmful ultraviolet (UV) radiation, thereby protecting life on the planet. However, drastic changes occurring in the Earth's magnetic field over geological timescales, termed geomagnetic excursions (GEs), can damage the ozone layer making it feasible for harmful UV radiation to penetrate deeper into the troposphere. This is here termed as the creation of 'UV window(s)' in the Earth's atmosphere. Direct observational evidence of the timing of formation of such UV windows during the GE events has been lacking and is needed to better understand the climate/environmental and societal impact of GEs in the past (and potentially in the future). Here, employing a novel geochemical tracer of UV radiation in polar ice core records, we detect the formation of such a UV window in the Earth's atmosphere ≈ 41.5 thousand years in the past during a period of severe magnetic field collapse which profoundly impacted life on the planet. We find the existence of this UV window had strongly materialized in the Southern Hemisphere. Overall, we

suggest that GEs can indeed create such UV windows, but their immediate effect might not be realized uniformly across the globe.

1. Introduction

The Earth's magnetic field, virtue of its dipole moment, shields life on the planet by deflecting much of the cosmic radiation reaching the Earth's surface (Merrillet et al 1983; Usoskin et al., 2008). However, variations in this dipole moment and as such the magnetic field have been noted to occur on geological timescales. Geomagnetic excursions are characterised by major changes in the Earth's magnetic dipole moment, lasting a few hundred to a few thousand years, and have been observed in the past (Herndon et al.,2020; Jackson et al., 2000; Simon et al., 2016; Valet et al., 2024). It is plausible that a weakened magnetic field could lead to the depletion of the stratospheric ozone layer through enhanced chemical effects in the upper atmosphere (Norval et al., 2007; Solomon et al., 1982, 1999; Winkler et al., 2008). Consequently, such an event could lead to the formation of 'UV window(s)' thereby allowing the harmful UV rays (Cooper et al., 2021; Dasari et al., 2022; Mukhopadhyay et al., 2025; Solomon et al., 1999), which otherwise would have been absorbed by the ozone layer, to penetrate deeper into the troposphere and, thus, towards the Earth's surface. Under such scenarios, the formation and persistence of UV windows would therefore be detrimental to both the environment and life on the plane (Cooper et al., 2021; Mukhopadhyay et al., 2025).

Studying past events of magnetic field collapse might hold the key to an improved understanding of the formation of UV window(s)(Cooper et al., 2021; Channell et al., 2019; Dasari et al., 2022; Valet et al., 2010). The period between ≈ 42 ka BP and ≈ 41 ka BP (thousand years before present), wherein the intensity of the Earth's magnetic field decreased by more than 80 % and then partially recovered (Valet et al., 2024), represents one of the most significant changes in the magnetic dipole moment (Cooper et al., 2021; Channell et al., 2019; Simon et al., 2007; Valet et al., 2024) (Figure 1a). This event, known as the Laschamp Geomagnetic Excursion (LGE), was a global and synchronous

71 event observed in many lavas of similar ages in New Zealand and California (Nowaczyk et al., 2025;
72 Valet et al., 2024) and highlighted in marine stratigraphic records (Valet et al., 2010) and ice-core
73 records from Greenland and Antarctica (Raisbeck et al., 1997, 2017; Yiou et l., 1999). Moreover, this
74 event is particularly intriguing and important because it has been proposed to explain global climatic
75 shifts during this period that yield to major environmental changes and life extinction (Cooper et al.,
76 2021; Valet et al., 2010). For instance, the LGE has been attributed as a contributing factor for the
77 subsequent disappearance of the Neanderthals (Cooper et al., 2021; Valet et al., 2010) contemporaneous
78 with this period, despite the notion being extensively debated (Picin et al., 2021; Hawks 2021). As such,
79 the LGE event represents a compelling case study for the formation and existence of UV window(s) in
80 Earth's atmosphere.

81 Mostly climate proxies and modelling works have been used to study the instances of increase
82 in UV influx in connection to the thinning/depletion of the ozone layer in the Earth's past (Hodson et
83 al., 2005; Marshall et al., 2020). Recently, fingerprinting sulfur-isotope anomalies recorded in Antarctic
84 ice-core sulfate records has shown promise in being able to observationally trace ozone layer depletion
85 events in the past (Dasari et al., 2022). In general, such isotopic anomalies are only ever recorded in
86 polar ice-core records during stratospheric volcanic eruptions wherein the plumes reach altitudes above
87 the ozone layer (Baroni et al., 2007; Burke et al., 2019; Gautier et al., 2019; McConnell et al., 2017;
88 Savarino et al., 2003). Subsequently, through a series of photochemical reactions involving UV
89 wavelengths between 190 and 250 nm and oxidation kinetics of S-bearing species such as sulfur dioxide
90 (SO_2) or carbonyl disulfide (CS_2), the synthesized sulfur-mass independent fractionation (S-MIF)-
91 bearing sulfate aerosols get deposited in the polar ice (represented by '$\Delta^{33}S$', also referred to as 'sulfur-
92 isotope anomaly', in ice-core sulfate isotope measurements; see Methods) (Farquhar et al., 2000;
93 Gautier et al., 2018; Hattori et al., 2013; Ono et al., 2017; Whitehill et al., 2015). However, it is logical
94 to envisage that in the event of a sustained depletion of the ozone layer occurring over hundreds of
95 years, such as during geomagnetic excursion events, the UV rays would penetrate towards Earth's

surface, thereby leading to the production of S-MIF-bearing sulfate aerosols in the troposphere during such periods (Figure 1). Consequently, the geochemical imprint of UV window(s) from ozone layer depletion could be found during such corresponding periods in polar ice-core records (Dasari et al., 2022).

However, ice-core sulfur-isotope records had only ever been used to detect volcanic events in the past (e.g., Baroni et al., 2007; Burke et al., 2019; Gautier et al., 2019; McConnell et al., 2017; Savarino et al., 2003) limiting the possibility of such a pursuit to trace UV windows using this geochemical tool. In this regard, our pilot study pioneering the application of sulfur isotope anomalies in polar ice-core records for a renewed purpose of tracing UV window(s) (Dasari et al., 2022) had recently investigated the period of ≈ 41.5 ka BP to ≈ 41.2 ka BP of the LGE event i.e., the reversed polarity phase (Figure 1a). During this period the partial recovery of the magnetic field had commenced, and the study found evidence for sulfur isotope anomalies in ice-core record not associated with any stratospheric volcanic influence, hinting the possibility of the existence of a UV in the Earth's atmosphere during the LGE event. However, direct evidence of the timing of the formation, the overall period of existence and above all, the globality of the UV window(s) during the LGE event is still lacking. These are crucial aspects which need investigating as the UV-influx from the LGE event may have profoundly impacted life on the planet (Cooper et al., 2021; Channel et al., 2019; Valet et al., 2010).

In this study, to test the timing of the formation, period of existence and globality of the UV window(s) during the LGE event, we provide a new record of sulfur-isotope anomalies ($\Delta^{33}S$) by sampling ice-cores from both Antarctica (Figure 2; see also Table S1 in Supporting Information) and Greenland (Figure 3; Tables S2-S3 in Supporting Information) with a focus on the weakened magnetic field phase (≈ 42 ka BP and ≈ 41.5 ka BP; Figure 1a) of the LGE event. We couple this with the re-analysed S-isotope record (see Methods) of the same Antarctic ice-cores from the pilot study (Dasari et al., 2022) for the reversed polarity phase (≈ 41.5 ka BP to ≈ 41.3 ka BP; Figure 1a) to overarchingly

explore the link between magnetic field collapse and recovery over the investigated 700-year period of the LGE event, and the concomitant changes in the stratospheric ozone layer in the Earth's past.

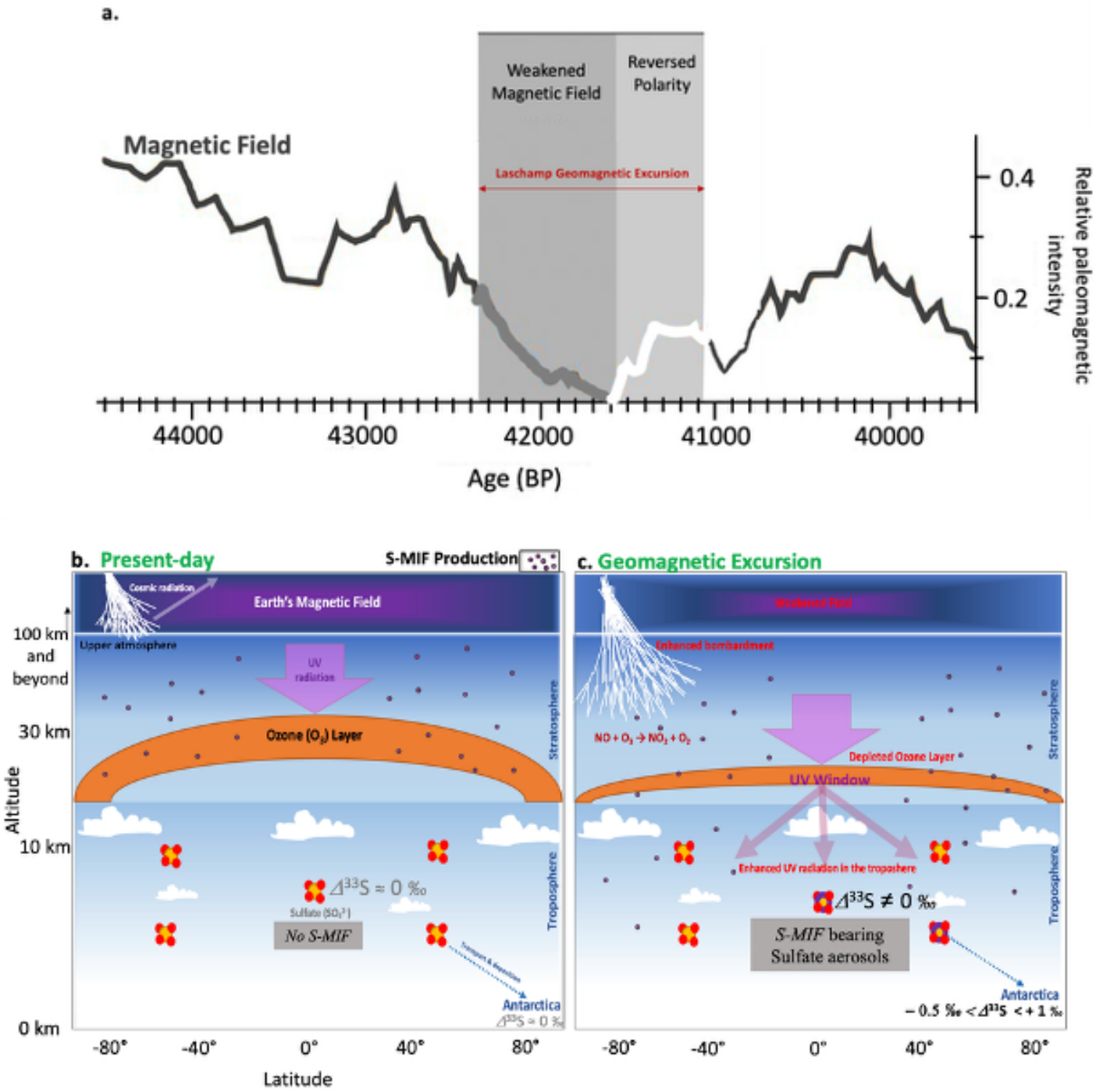

Figure 1. S-MIF based investigation of a UV window during geomagnetic excursion events. (A) The evolution of the paleomagnetic intensity during the Laschmap geomagnetic excursion event is shown.

(B) Schematic of tropospheric S-isotope imprint without UV window. Most of the isotopic fractionation mechanisms for sulfur fractionate isotopes are in proportion to their mass, according to the so-called "mass dependent" fractionation laws (MDF). For MDF, one can write $\delta^{33}S \approx 0.515 \times \delta^{34}S$ (for its linear approximation), If $\Delta^{33}S \neq 0$, then it is referred to as "mass-independent" fractionation (MIF) (Farquhar et al., 2000; Gautier et al., 2018; Hattori et al., 2013; Ono et al., 2017; Whitehill et al., 2015). In the present atmosphere, the presence of the ozone layer along with an intact geomagnetic field prevents the creation of such large-scale fractionation i.e., $\Delta^{33}S = 0$ ‰ in modern day atmospheric sulfate in polar ice. **(C)** Schematic of tropospheric S-isotope imprint without UV window. During the Geomagnetic Excursion events creation of a UV 'window' could lead to deeper penetration of UV radiation towards the Earth's surface. The UV-induced photochemistry can then generate measurable S-MIF splits in tropospheric sulfate produced from S-containing compounds such as SO_2, CS_2, which can be detected in polar ice-core sulfate records for the corresponding periods (Dasari et al., 2022).

2. Materials and Methods

2.1 Ice-core sulfate sampling, isolation and isotope measurements

High-resolution sampling of ice-cores was conducted by cutting ~3 cm slices along the wings of the cores. Outside edges of the ice-cores were scraped clean, and ice-core slices were then decontaminated by rinsing the ice with ultrapure water (Milli-Q, Millipore Corp.) and, finally, melted and filtered at 0.45 μm. Major water-soluble ions were measured by ion chromatography (Metrohm IC Professional 850), each slice requiring 2 ml of the sample. The quality assurance of the analytical data (within 5 %) was ascertained by preparing standard stock solutions from analytical grade reagents and salts, and reported concentrations were suitably blank corrected. Depending on the sulfate concentrations, samples were pooled (providing ~ 10-year time resolution) and sulfate was then isolated using ion chromatography-based fraction separation at IGE as described elsewhere (Gautier et al., 2019).

The sampled Antarctic ice-cores (core: Vostok 3G; 78.46°S 106.83°E) were from 611-615 m in depth (≈ 41.6 to ≈ 42 ka BP in age; AICC 2023 chronology (Bouchet et al., 2023); Table S1 in Supporting Information) whereas for the discrete sub-sampled Greenland ice-cores (core: NGRIP; 75.10°N, 42.32°W) this was 2126–2129 m in depth (≈ 41.5 to ≈ 41.7 ka BP in age; AICC 2023 chronology; Table S2 in Supporting Information). The reason for the partial overlap was the limited availability of sample as well as the intention to cover the overlapping period of the lowest magnetic field intensity (Figure 1) in the dual-polar ice-core samples (see also age transfer function in Table S3 in Supporting Information). This new Antarctic ice-core (site: Vostok 3G) sulfate record was then coupled with the data from the pilot study (for the 'non-volcanic' sulfate period alone; see Discussion) wherein sampled cores were from 607-611 m in depth (≈ 41.3 to ≈ 41.6 ka BP in age; AICC 2023 chronology) (Dasari et al., 2022). The pilot study also analyzed the period 41.2 to 41.3 ka BP which was dominated by 'volcanic' sulfate and was therefore not used in the merged record here.

The isolated sulfate extracts were then analyzed for S-isotopes at CRPG with the Neptune Plus MC-ICP-MS (Thermo Fisher Scientific Neptune Plus) following well-established protocols for small sample analysis (Paris et al., 2013, 2014, 2024). The MC-ICP-MS was coupled with a desolvation membrane (Aridus II, Cetac) which reduces the interference of oxides and hydrides on the masses ^{32}S, ^{33}S, and ^{34}S and hence increases the sensitivity to the signal. The samples were analysed by standard-sample bracketing using an in-house Na_2SO_4 standard to correct for instrumental isotopic fractionation (Paris et al., 2024). Before introducing the sample to the instrument, the sulfate extracts were evaporated to dryness, resuspended in 5 % HNO_3, and NaOH was added to the sample to match the concentration and matrix of the in-house Na_2SO_4 bracketing standard with a concentration of 40 µmol/L (Dasari et al., 2022b). As part of quality control, the bracketing standard was measured as a sample with decreasing sulfate concentration, showing no bias induced by sulfate concentration as long as Na concentration matches that of the bracketing standard, in agreement with previous studies (Dasari et al., 2022a, 2024). Each sample was run a minimum of four independent times, usually five, with each

run making fifty measurements and a sulfate concentration between 20 and 40 µmol/L. The reported values (Tables S1 in Supporting Information) are given as an average of at least five independent measurements on the Neptune for a given sample. This analytical error (usually < 0.05 ‰, 1σ) is an improvement from previous MC-ICP-MS-based studies (Dasari et al., 2022a, 2022b, 2024; Paris et al., 2013, 2014, 2024) as samples are run (i) at a higher concentration (up to 40 µmol/l instead of less than 20 µmol/L) and (ii) 5 times instead of 2, respectively. The error accounts for instrumental reproducibility.

The triple sulfur isotopes (^{32}S, ^{33}S, ^{34}S) are reported relative to Vienna-Canyon Diablo Troilite (V-CDT). $\Delta^{33}S$ is here defined as $\delta'^{33}S - 0.515 \times \delta'^{34}S$, where $\delta'^{3x}S = \ln[(^{3x}S/^{32}S)_{sample}/(^{3x}S/^{32}S)_{standard}]$ (Hulston & Thode, 1965). The bracketing standard was calibrated against the international standard IAEA-S1 assuming $\delta^{34}S$ = -0.3 ‰ and $\delta^{33}S$ = -0.061 ‰ (and thus $\Delta^{33}S$ = 0.094 ‰). Further quality control was conducted using a secondary sulfur isotope reference material 'SMIF-1' which yielded a $\delta^{34}S$ value of 10.06 ± 0.14 ‰ and $\Delta^{33}S$ of 9.46 ± 0.14 ‰ (n = 5) in agreement with the reported $\Delta^{33}S$ = 9.54 ± 0.09 ‰ from five different laboratories worldwide (Geng et al., 2019). A seawater sample was also run further to ensure the precision and accuracy of the measurements. It yielded $\delta^{34}S$ and $\Delta^{33}S$ values of 21.14 ± 0.09 ‰ and 0.07 ± 0.12 ‰ (2 s.d., n=5), in agreement with previously published values (Paris et al., 2013, 2014, 2024). The seawater sample was purified at CRPG following a column chemistry method (Paris et al., 2013, 2014, 2024). Procedural blanks were also run with each set of samples. Overall, high-precision measurements of both $\delta^{34}S$ and $\Delta^{33}S$ were ensured during this investigation (Tables S1-S2 in Supporting Information).

2.2 Calculation of the non-sea salt (NSS)-sulfate isotopic signatures

The polar ice-core sulfate is a mix of sea water sulfate and atmospheric sulfate (from a -variety of sources). To isolate the atmospheric component, a sea-salt sulfate (SS) correction needs to be made

199 both for concentration and isotope ratios (e.g., Gautier et al., 2019). The concentration of SS present in
200 aerosols is usually estimated according to the relation:
201
202 $$[SO_4^{2-}]_{SS} = k\,[Na^+] \quad (1)$$
203
204 A k value of 0.25 is often used for this calculation in seawater, but in Antarctica, due to temperature
205 differences, the sea salt emitted from the sea ice surface is depleted in SO_4^{2-} relative to Na^+. As such,
206 lower values have been reported at various Antarctic sites (Alexander et al., 2003; Ishino et al., 2019),
207 e.g., at Dome C (0.16) and DDU (0.13), respectively. Therefore, a mean k value of 0.14 has been used
208 here.
209
210 Quantity of non-sea-salt (NSS) sulfate is then determined using the relation as in previous studies
211 (Gautier et al., 2019; Uemura et al., 2022):
212
213 $$[SO_4^{2-}]_{NSS} = [SO_4^{2-}]_M - [SO_4^{2-}]_{SS} \quad (2)$$
214
215 Where $[SO_4^{2-}]_M$ is the concentration of sulfate measured in the sampled ice-core
216
217 The isotopic composition of the NSS is then approximated using the following mixing equation:
218
219 $$\delta^{34}S_{NSS} \approx (\delta^{34}S_M - [1\text{-}X]\,\delta^{34}S_{SS})/\,X \quad (3)$$
220
221 where X is the proportion of NSS defined as $X = [SO_4^{2-}]_{NSS} / [SO_4^{2-}]_M$ and $\delta^{34}S_{SS}$ is the average isotopic
222 composition measured in seawater. This equation (3) can also be used to express the $\delta^{33}S_{NSS}$.
223

Finally, the $\Delta^{33}S_{NSS}$ is expressed (in per mil) as follow :

$$\Delta^{33}S_{NSS} = \delta^{33}S_{NSS} - \{[(\delta^{34}S_{NSS}) + 1]^{0.515} - 1\} \quad (4)$$

Note the data in the pilot study (concentrations and isotope values) were not corrected for contribution from sea salt. As such, in the merged record here (Table S1 in Supporting Information) the data from the pilot study was reanalyzed accounting for the sea salt correction as was done for the new record in the present study.

2.3 Source apportionment of polar ice-core sulfate

We consider three possible sources of sulfate in the polar ice core samples: marine biogenic (*bio*), volcanic (*vol*) and terrestrial (*terr*). Combining the source contributions is expected to yield the observed $\delta^{34}S_{NSS}$ as per the following equations:

$$f_{bio}\,\delta^{34}S_{bio} + f_{vol}\,\delta^{34}S_{vol} + f_{terr}\,\delta^{34}S_{terr} = \delta^{34}S_{NSS} \quad (5)$$

$$f_{bio} + f_{vol} + f_{terr} = 1 \quad (6)$$

where $f_{bio,vol,terr}$ and $\delta^{34}S_{\,bio,vol,terr}$ are the fractions and isotopic signatures attributable to of sulfate from the biogenic, volcanic and terrestrial sources, respectively. Here, we have used the values for $\delta^{34}S_{bio}$ = 18.8 ± 0.3 ‰ and $\delta^{34}S_{vol}$ = 4.1 ± 0.5 ‰ determined elsewhere (Kiyosu 1985; Jongebloed et al., 2023). $\delta^{34}S_{ter}$ has been shown to vary regionally, as such we have used a global average of 4.4 ± 4.5‰ (Burke et al., 2018).

A Bayesian mixing model was implemented in PyMC (Python) building on previous works (Dasari et al., 2020, 2021, 2022b, 2024) to quantify the proportional contributions of these three sulfur sources—'*bio'*, '*vol'* and '*terr*'—to observed $\delta^{34}S$ values, where each source endmember was treated as a hierarchical random variable with a normal prior distribution defined by its mean and standard deviation to propagate endmember uncertainty through the model. For each sample, the source fractions (f_bio, f_vol, f_terr) were assigned a Dirichlet prior with $\alpha = [1,1,1]$, ensuring non-negativity and sum-to-one constraints while providing weakly informative regularization. The predicted $\delta^{34}S$ for each sample was calculated as the weighted sum of the three endmembers, and the likelihood was defined as a normal distribution centered on this predicted value with a standard deviation equal to the quadrature sum of the sample-specific analytical uncertainty (ranging from 0.02 to 0.28‰) and a 0.05‰ systematic uncertainty term to account for unmodeled processes. Posterior distributions were estimated using Markov Chain Monte Carlo (MCMC) simulation with four independent chains, each running 10,000 sampling iterations after 2000 warmup iterations, yielding 15,000 posterior draws per parameter. Convergence was assessed using the Gelman-Rubin R-hat statistic (<1.05 for all parameters) and effective sample size (>400), while posterior predictive checks confirmed adequate model fit. The output provides for each sample the mean source fractions, standard deviations, and 95% highest density intervals (HDI) for each source, allowing comprehensive uncertainty characterization that integrates analytical measurement error, endmember variability, and mixing model uncertainty into probabilistic source contribution estimates (Tables S4-S5 in Supporting Information). Further information on the model and the uncertainty estimation can be found elsewhere (Dasari et al., 2022b, 2024)

3. Results and Discussion

In the Antarctic ice-core sulfate record, considerable variability was found in the sulfate concentrations and the corresponding isotopic signals. The total measured sulfate concentrations, $\delta^{34}S$, and $\Delta^{33}S$ values varied from 100 to 900 ng g^{-1}, from 4 ‰ to 16 ‰, and from -0.1 ‰ to +0.5 ‰, respectively. The estimated average sea-salt sulfate fraction and sulfate flux were 10 ± 6 % and 3 ± 2 kg km^{-1} yr^{-1} over the sampled event, respectively. Upon correcting the record for the sea salt fraction, the non-sea salt sulfate concentrations ($[SO_4^{2-}]_{NSS}$), $\delta^{34}S_{NSS}$, and $\Delta^{33}S_{NSS}$ values varied from 80 to 830 ng g^{-1}, from 3.5 ‰ to 15 ‰, from -0.50 ‰ to +1 ‰, respectively (Figure 2; see also Table S1 in Supporting Information).

Here, the $\delta^{34}S_{NSS}$ values were found to be mostly stable with average value being 13 ± 2 ‰, apart from the period between 42 ka BP and ≈ 41.9 ka BP when the average $\delta^{34}S_{NSS}$ was 7 ± 4 ‰ (Figure 2). Changes to the $\delta^{34}S_{NSS}$ values were, however, concomitant with changes in the average $[SO_4^{2-}]_{NSS}$ which increased from 190 ± 70 ng/g (≈ 41.9 to 41.3 ka BP) to 320 ± 170 ng/g (≈ 42 and 41.9 ka BP), respectively (Figure 2). This contrasts with the $\Delta^{33}S_{NSS}$ values with maximum variability found in the period when both the $\delta^{34}S_{NSS}$ and $[SO_4^{2-}]_{NSS}$ were relatively stable (Figure 2). This amplitude of variations in the $\Delta^{33}S_{NSS}$ values in the weakened magnetic field phase (-0.53 ‰ to +0.96 ‰; new record) was found to more pronounced than in the reversed polarity phase (+0.04 ‰ to +0.16‰; reanalysed pilot study record) (Figure 2). Overall, 72 ± 19% and 22 ± 20% of the non-sea salt sulfate in Antarctic ice-cores during this period was sourced from biogenic and volcanic emissions, respectively, with the remaining 6 ± 4% was sourced from terrestrial sources (see Methods; Table S4 in Supporting Information).

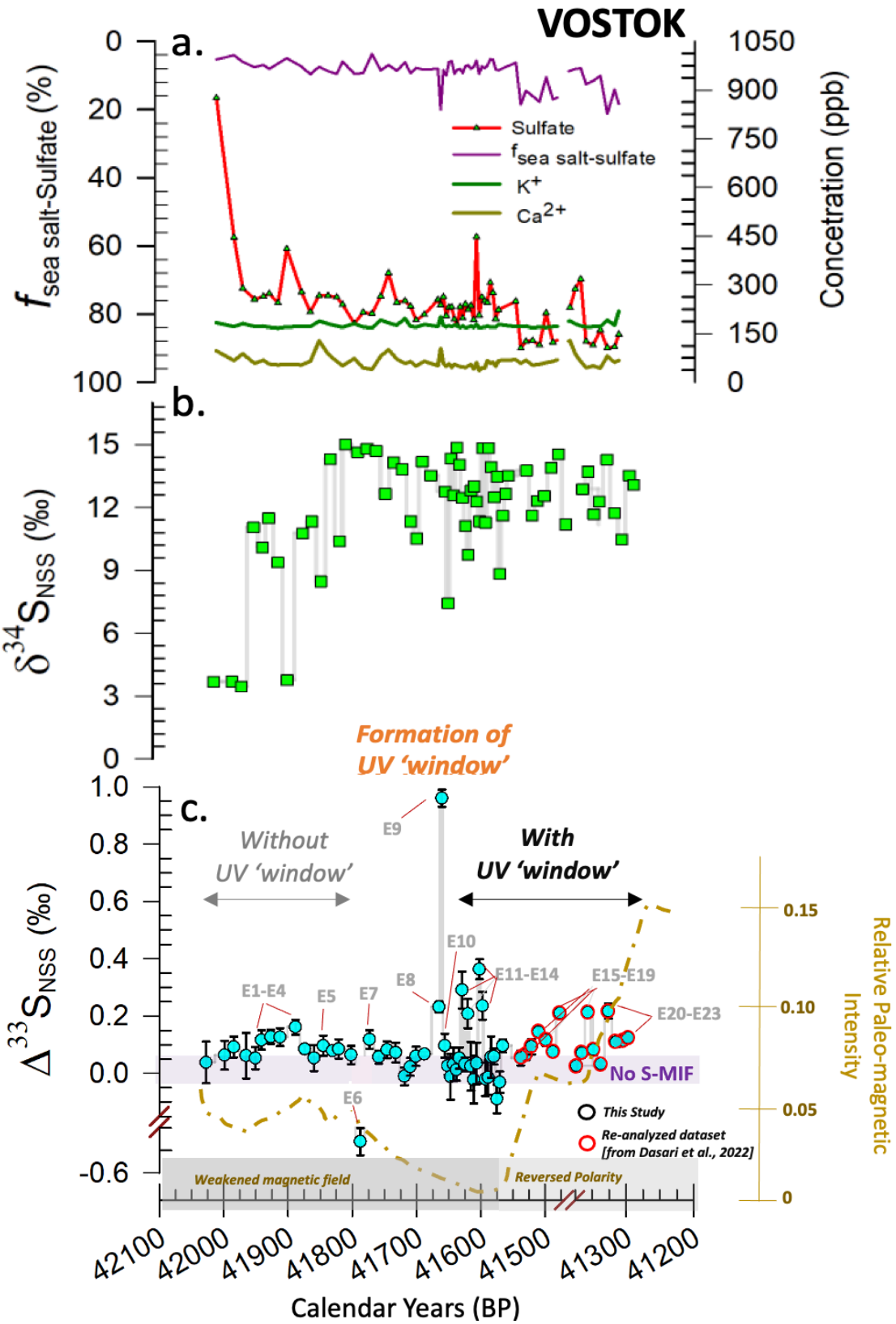

Figure 2. The evolution of Antarctic ice-core sulfate dynamics and isotopic signatures during the investigated 700-years of the Laschamp Geomagnetic Excursion event. (A) Sulfate along with other water-soluble ion concentrations are reported. The non-sea-salt sulfate fraction is shown. **(B)** $\delta^{34}S_{NSS}$

values are reported. **(C)** $\Delta^{33}S_{NSS}$ values are reported from Antarctic ice-cores (see also Methods, Figure S1 and Tables S2-S3 in Supporting Information) along with the periods of the formation and existence of the UV window during the event. The relative paleomagnetic intensity (from Figure 1a) is shown (dotted line) here for the analysed period. E1-E23 mark the events wherein anomalous sulfate ($\Delta^{33}S\neq0$) was detected during the investigated period. Note (in A - C) the data from this study (≈ 42 to ≈ 41.5 ka BP) is merged with the reanalysed data from a previous study (Dasari et al., 2022) for the periods ≈ 41.5 ka BP to ≈ 41.2 ka BP (see Methods) to create the 700-year record. The distinct phases of the magnetic field evolution (see Figure 1) during this period are shown. The AICC2023 chronology has been used (Bouchet et al., 2025).

In Greenland ice-core sulfate record, measured for the overlapping period of the magnetic field collapse between ≈ 41.8 and ≈ 41.5 ka BP, the estimated average sea-salt sulfate fraction and sulfate flux were 17 ± 3 % and 60± 20 kg km^{-1} yr^{-1} over the sampled event (Figure 3; see also Table S2 in Supporting Information). Upon correcting the record for the sea salt fraction, the average non-sea salt sulfate concentrations ($[SO_4^{2-}]_{NSS}$), $\delta^{34}S_{NSS}$, and $\Delta^{33}S_{NSS}$ values were 250 ± 90 ng/g, from 4.2 ± 1 ‰, and +0.08 ± 0.01 ‰, respectively (Figure 3). Overall, 14 ± 9% and 62 ± 8% of the non-sea salt sulfate in Greenland ice-cores during this period was sourced from biogenic and volcanic emissions, respectively, and the remaining 24 ± 8% was sourced from terrestrial sources (see Methods; Table S5 in Supporting Information). Taken together, the findings show considerable shifts in $\Delta^{33}S_{NSS}$ in the southern polar ice-core record alone and a lack of similar response in the northern polar ice-core record. This is a notable feature of the bi-polar ice-core sulfate record for the LGE event, and an aspect that has not yet been found in other geochemical proxies from this period (Cooper et al., 2021; Reisbeck et al., 2017).

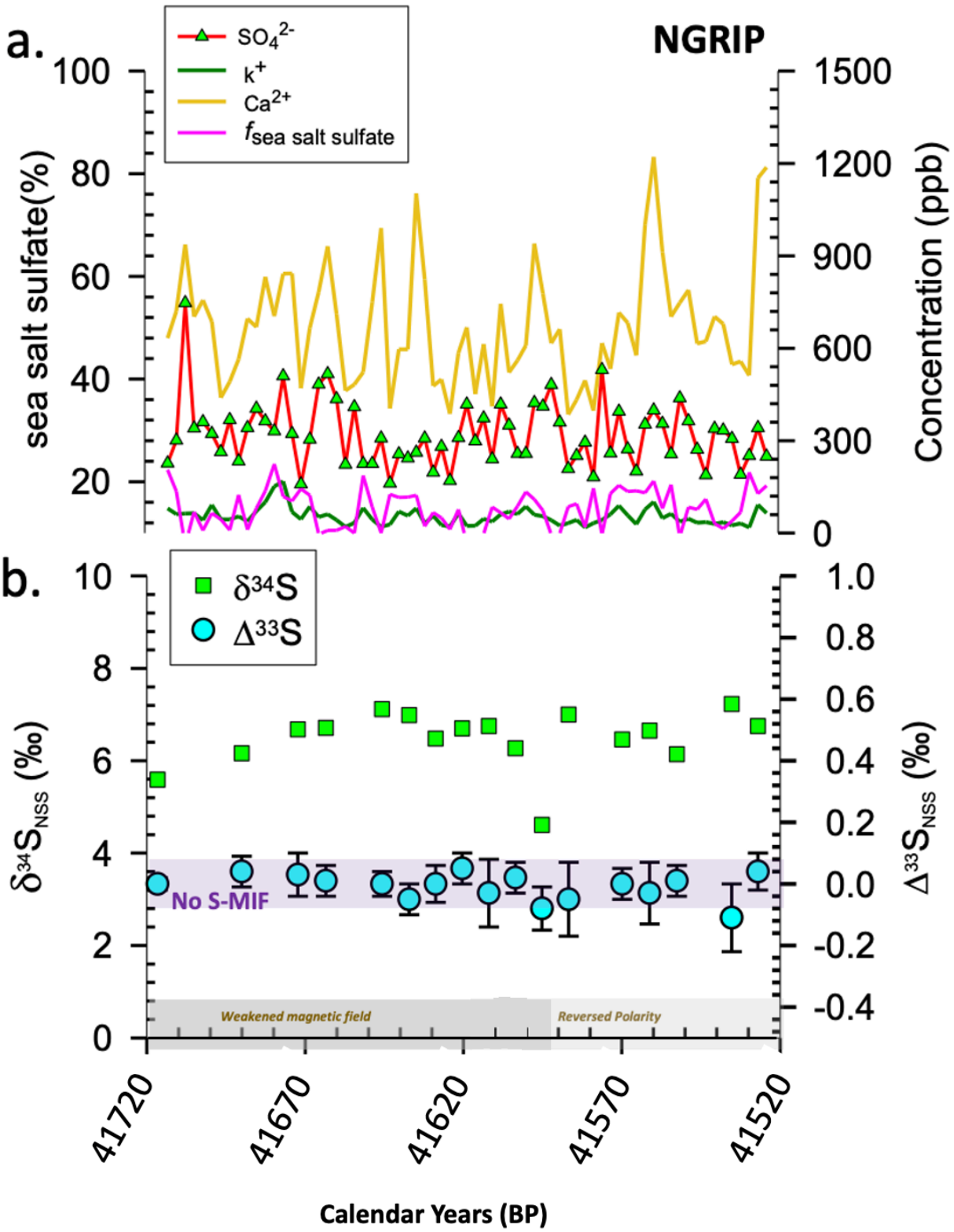

Figure 3. The evolution of North Greenland ice-core sulfate characteristics during the Laschamp Geomagnetic Excursion event for overlapping period of UV-window formation. **(A)** Sulfate along with other water-soluble ion concentrations are reported. The non-sea-salt sulfate fraction is shown.

(B) $\delta^{34}S_{NSS}$ values and $\Delta^{33}S_{NSS}$ values are reported from NGRIP ice-cores (see also Methods and Tables S2-S3 in Supporting Information). The distinct phases of the magnetic field evolution (see Figure 1) during this period are shown.

3.1 Investigating the origin of the observed S-MIF in the ice-core sulfate record

For the purpose of identifying the existence of a UV window, knowledge of the origin of S-MIF in ice-core sulfate—with the distinction of stratospheric volcanic sulfate—in the record is crucial (Dasari et al., 2022). During volcanic eruptions, the SO_2 oxidation kinetics imprinted in ice-core sulfate is such that the sulfur-isotope anomalies follow a cyclic pattern — changing from positive $\Delta^{33}S$ values at the beginning of the sulfate deposition to negative values at the end (Baroni et al., 2007; Burke et al., 2019; Gautier et al., 2018. The volcanic sulfate is superimposed on the marine-generated sulfate forming the continuous, low-concentration background (Baroni et al., 2008; Cole-Dai et al., 2021; Pearson et al., 2022). The volcanic deposition is often marked by an increase in sulfate concentrations and a corresponding decrease in $\delta^{34}S_{NSS}$ values in the ice-core record (Baroni et al., 2007; Burke et al., 2019; Baroni et al., 2008; Cole-Dai et al., 2021; Gautier et al., 2019; Pearson et al., 2022; Savarino et al., 2003).

Other than this aspect, the triple S-isotope signatures also offer the possibility to better understand the stratospheric volcanic origin of the observed S-MIF in ice-core sulfate record (Baroni et al., 2007; Gautier et al., 2019). As a consequence of the well-established stratospheric SO_2 oxidation kinetics and sedimentation dynamics, the $\Delta^{33}S_{NSS}$ versus $\delta^{34}S_{NSS}$ slope is constrained to be 0.09 (σ = 0.02) (Gautier et al., 2018) (Figure 5). Prior to this work, the validity of the slope had only been tested for ~2500 years of recorded polar ice-core S-MIF history (Gautier et al., 2019). As part of the pilot study covering the reversed polarity phase of the LGE event, a stratospheric volcanic eruption was recorded during ≈ 41.2 ka BP (Dasari et al., 2022). This allows for an opportunity to further test the validity of the slope for 41 millennia ago, which notably is found to be in alignment with the previously

established slope (Figure 5), thereby asserting the validity of the slope as a means to delineate stratospheric volcanic influence on the observed S-MIF bearing sulfate in the ice-core record.

In the present study, the observed triple S-isotope systematics between 42 ka BP and ≈ 41.9 ka BP, accompanied with high sulfate concentration is suggestive of a stratospheric volcanic influence. However, we note the time resolution of the ice-core samples was ~15 and 20 years, as such detecting any cyclic S-MIF pattern from volcanic eruptions (as opposed to in studies with much higher time resolution wherein such pattern was detected) was highly unlikely. Yet, S-MIF was detected in 3 out of 8 samples during this period (and more in the remainder of the record as discussed later; SI Table S1). Here, we refer to the samples with detectable S-MIF during the LGE as 'Events (E; Figure 2)' and explore these further : the $\Delta^{33}S$ values in the 3 events (marked 'E1-E3'; Figure 2) displayed an enrichment in $\delta^{34}S_{NSS}$ concomitant to the sulfate becoming dominated with volcanic origin (Figure 4), and were in alignment with observed volcanic slope (Figure 5). This is in line with the established pattern of S-MIF from stratospheric volcanic eruptions and could rather be linked to extratropical volcanoes (Burke et al., 2019). During such eruptions the initial transport of the volcanic plume is expected to happen in the troposphere which could also lead to a depletion in the $\delta^{34}S_{NSS}$ and concomitant increase in sulfate concentration in ice-core sulfate (as observed in the first 50 years of the record; Figure 2), with the S-MIF bearing sulfate approaching later after the event (EI-E3; Figure 5). However, such volcanic events last only a few years (Burke et al., 2019) but here the sulfur-isotope anomalies in 'E1-E3' were observed on multi-decadal time resolution (spanning 60 years) which is not expected from a 'volcanic only' process. As this period is concomitant with the abrupt changes in the magnetic field (Figure 1a), it is therefore plausible that a secondary process could have been causing this sustained detection of S-MIF bearing sulfate in the troposphere during this period. Further investigation of such events in the remainder of the record could yield valuable insights into this secondary process.

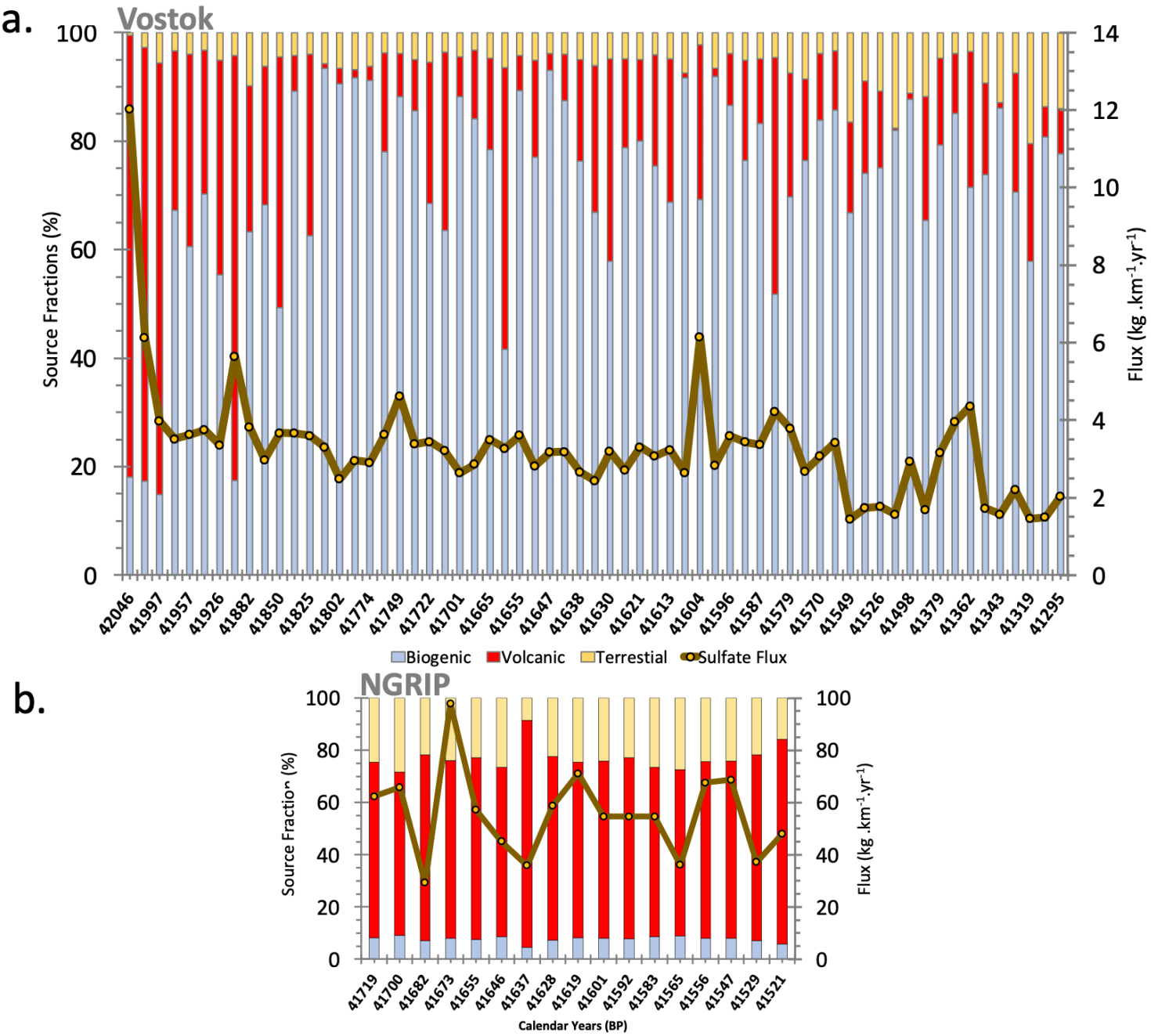

Figure 4. Source apportionment of polar ice core sulfate during the Laschamp Geomagnetic Excursion event. The observed $\delta^{34}S_{NSS}$ values are used to apportion the ice-core sulfate into marine biogenic, volcanic and terrestrial source fractions (see Methods) for Vostok (A) and NGRIP (B) samples used in this study (see Tables S1-S2 in Supporting Information). Sulfate flux computed for both these locations is also shown.

372 In fact, the triple S-isotope signatures of the remaining events ('E4-E16'; Figure 5) in the period
373 between ≈ 41.9 ka BP and ≈ 41.5 ka BP are not consistent with the volcanic slope even if we consider
374 uncertainties. This is also the case for the reanalysed $\Delta^{33}S$ values between ≈ 41.5 ka BP and ≈ 41.3 ka BP;
375 'E17-E23' (from reanalysed data from the pilot study; Figures 2 and 5). Furthermore, the sulfate concentrations
376 and $\delta^{34}S_{NSS}$ values for these periods (Figure 2) are comparable to that of the previously reported background
377 values across different sites in Antarctica, such as at Dome C and the South pole (concentration of 80 ± 20
378 ng/g, $\delta^{34}S_{NSS}$ of 14 ± 2 ‰) (Jourdin et al., 2002; Legrand et al., 2017). This indeed implies that S-MIF bearing
379 tropospheric sulfate being present in 'background' Antarctic atmosphere between ≈ 41.9 ka BP and ≈ 41.3 ka
380 BP, i.e., for the combined 600-year period of the LGE event.

381 The finding of S-MIF in tropospheric sulfate aerosols across a period of 600-years is intriguing. This
382 is because an estimated ~ 80% (20%) of the sulfate in 'E4-E23' was sourced from marine biogenic (volcanic)
383 emissions (Figure 4), which in general are not found to be associated with significant S-MIF ($\Delta^{33}S_{biogenic} \leq 0.05$
384 ‰; $\Delta^{33}S_{tropospheric\ volcanoes} \sim 0$ ‰) (Alexander et al., 2003; Baroni et al., 2008; Burke et al., 2019). This is also
385 evidenced in the year-round investigation of atmospheric sulfate aerosols in Antarctica, wherein the reported
386 $\Delta^{33}S$ was ≈ 0.01 ‰ on average for samples collected at both Dome C and Dumont d'Urville research stations
387 (Ishino et al., 2019). Likewise, sulfate formed in the troposphere and found in the snow or soil of Antarctica
388 has never shown any sulfur isotope anomaly either (Alexander et al., 2003). The amplitude of isotopic shifts
389 ($\Delta^{33}S$ varying between -0.5 ‰ to +1 ‰) for marine-biogenic and tropospheric volcanic emissions sourced
390 sulfate are therefore unique from the perspective of S-MIF based investigations in pristine environments. This
391 potentially implicates deeper penetration of UV radiation in the troposphere as the secondary process
392 generating S-MIF (other than stratospheric volcanic influence potentially for 'E1-E3'; Figure 5) during the
393 investigated period of the LGE event.

394

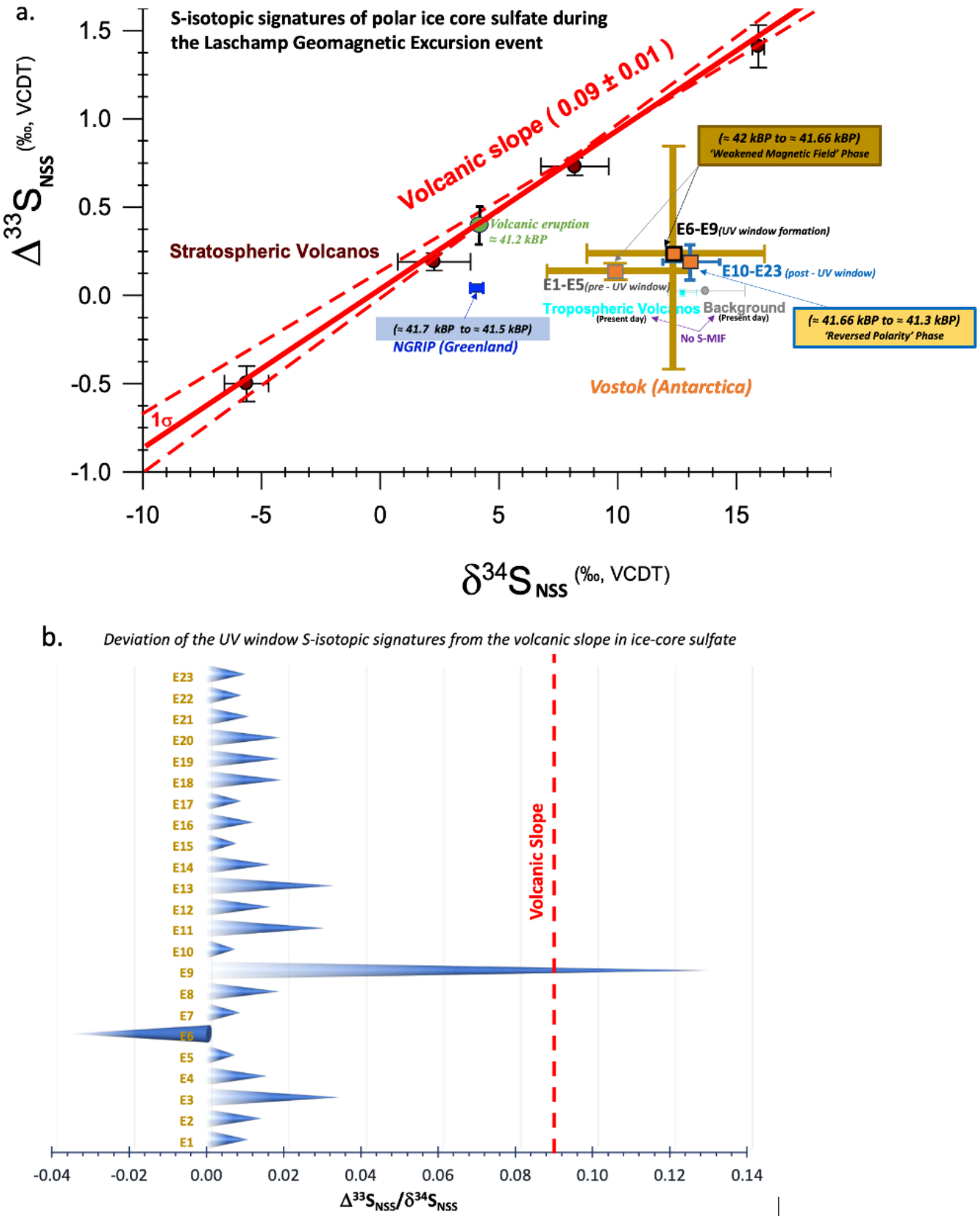

Figure 5. Triple-isotope-based deconvolution of the S-MIF signals during the Laschamp geomagnetic excursion event. (A) Five stratospheric volcanoes (circles), Kuwae, Samalas, 1809 UE, 1259 UE, and

Agung, are shown. Also shown is the 'volcanic' eruption detected during the Laschamp geomagnetic excursion event in the pilot study[11] showing the validity of the volcanic slope during the corresponding period as well. The isotopic signatures of previously reported tropospheric volcanoes and background sulfate are shown. The averaged UV window isotopic signatures (E1-E23) in various phases are shown. (B) Deviation of the events E1-E23 from volcanic slope is shown.

An increase in stratospheric tropospheric transport of airmasses is a possibility brining in sulfate bearing S-MIF and the existence linked to a DO event. Such an event could not have spanned the An influx of UV radiation towards the Earth's surface is possible through the thinning/destruction of the ozone layer during geomagnetic excursions as shown in Figure 1b, which is likely the case during the investigated period. Taken together, the detection of S-MIF bearing sulfate in background Antarctic conditions during the LGE event here unequivocally confirms the presence of a UV window during ≈ 41.9 ka BP to ≈ 41.3 ka BP period. We postulate that while the annually forming ozone hole over Antarctica for short duration (few months) does not show any measurable S-MIF in ice-core sulfate, geomagnetic excursions in the past can ideally be traced in Antarctic ice-core records. While mostly positive sulfur-isotope anomalies values were observed during the LGE event, it is plausible that the negative S-isotopic anomalies created in the process are stored in other S-reservoirs (e.g., 'COS', 'SO', 'CS_2', CH_3SO3_H) and as such remain undetected in the present ice-core 'sulfate' isotopic record (Colman et al.,1996; Wanatabe et al., 2009; Shaheen et al., 2014). Some reports have also suggested detection of only positive anomalies in ice-core sulfate during volcanic eruptions and the negative anomalies were either lost, not detected in those ice-cores or remain less transported to Antarctica in general (Baroni et al., 2007; Gautier et al., 2016. It is here speculated that this remains a possibility in the present sampling scheme as well.

3.2 Testing the globality of the UV window

The geographical representativeness of the sampled ice-cores can be used to investigate the globality of the UV window. While the sampled Greenland ice-core sulfate record here is limited to 200-years, this overlapping period (≈ 41.7 ka BP and ≈ 41.5 ka BP; SI Table S3) with the Antarctic ice-core records maximizes the possibility for ascertaining the globality of the UV window (given the concomitance with the lowest relative paleomagnetic intensity; see Figure 1a). Long-term volcanic records have shown the detection of 'global' events in bi-polar ice-core sulfate records (Gautier et al., 2019; Lin et al., 2022; Sigl et al., 2013; Svensson et al., 2020). In general, a global volcanic event is often found to be synchronous in bi-polar ice-core sulfate records. In the present Antarctic record here, initially between ≈ 42 and 41.9 ka BP we find fewer and sporadic events (E1-E3) of S-MIF bearing sulfate in Antarctica (Figure 2). Immediately following this period, striking positive (E6) and negative peaks (E9) in sulfur-isotope anomalies are detected between ≈ 41,787 BP and ≈ 41,659 BP (Figure 2), which are synchronous with the weakest magnetic field intensity (Figure 2) and suggests the possibility of the UV window being formed in the Earth's atmosphere during these ~ 100 years of the LGE event. Beyond 41,659 BP and into the reversed polarity phase of the LGE event, the sporadicity in detecting sulfur-isotope anomalies in Antarctic ice-core record also decreases and more events are detected (E10-E14 still in the weakened magnetic field phase and E15-E23 in the reversed polarity phase; Figure 2) implying the sustained presence of the UV window in the Earth's atmosphere. Further investigation into background sulfate ≈ 41 ka BP in the pilot study revealed no detectable S-MIF implying that the UV window (Dasari et al., 2022a), and thereby the ozone layer, could have plausibly recovered by that period, in line with the regaining of the magnetic field intensity (Figure 1a). This is therefore potentially new evidence regarding the 'timing' of formation of a UV window in the Earth's atmosphere during the LGE event.

Unlike the Antarctic record, the observed ice-core sulfate dynamics in Greenland during the sampled overlapping period of the LGE event showed no measurable S-MIF in background sulfate in

447 the north (Figure 3). The absence of the discernable S-MIF in northern polar ice-core records can be
448 linked to the several putative possibilities which we explore in detail:

449 (i) A higher snow accumulation rate, and thereby the sulfate flux (Figure 4), in Greenland
450 compared to Antarctica could lead to dilution of the S-MIF signal (Leonard et al., 2004; Neilsen
451 et al., 2014). This is possible only under the assumption that most of the sulfate transported to
452 Greenland was predominately formed from mass-dependent fractionation (MDF) pathways. But
453 events E5-E23 show that 'background' tropospheric sulfate (detected across the 600-year
454 period) was S-MIF bearing during this period. There is no clear way to apportion the fraction
455 of MIF-bearing and MDF-bearing sulfate in the sulfate flux.

456 (ii) Alternatively, the $\delta^{34}S_{NSS}$ values of Greenland ice-core sulfate suggest that sulfate could have
457 been sourced largely from continental origin (Jonegebloed et al., 2023) relative to the marine
458 biogenic emissions (Figure 4). Conflicting reports have emerged regarding S-MIF in continental
459 sulfate with recent studies suggesting such possibility exists in urban locations perhaps
460 speculatively linked to the role of organics whereas chamber studies in the past have advocated
461 against this process (au Yang et al., 2019; Dasari et al., 2022b, 2024). Moreover, combustion-
462 associated sulfate aerosols in biomass burning have also displayed S-MIF. Sulfate from biomass
463 burning has been mostly associated with positive $\Delta^{33}S$ anomalies (Dasari et al., 2023) whereas
464 from biofuel (e.g., wood) burning with negative $\Delta^{33}S$ anomalies (Han et al., 2017; Pei et al.,
465 2026). The $\delta^{34}S$ value of such sources are rather similar to the ones found in the Greenland ice-
466 core sulfate record, yet, lacking evidence of any S-MIF imprint. Other than this source, the
467 remaining sulfate was primarily sourced from a mixture of tropospheric volcanic and marine
468 biogenic emissions (Table S2 in Supporting Information and Figure 4). As found in the
469 Antarctic record (Figure 5), sulfate from a mix of these sources did display S-MIF during the
470 investigated period of 600 years of the LGE event linked to the presence of a UV window.

(iii) While accounting for the role of atmospheric deposition and dynamics during the LGE event remains beyond the scope of the present study, it is plausible that the S-MIF bearing sulfate could arrive at the NGRIP site later than the period investigated here (Gautier et al., 2016). However, given the synchroneity between the collapse of the magnetic field and the events E6-E9 (Figure 2), we argue that such a geochemical imprint should have been witnessed in the northern ice core record either instantaneously or within the ~100-year period of covered by E6-E9, as supported by bi-polar records of other cosmogenic tracers during this period (Reisbeck et al., 2007, 2017) . Furthermore, during events of climate transitions such as the between Greenland Interstadial and stadial periods, an increase in stratospheric tropospheric transport (STT) has been reported (Geng et al., 2017). Here, the subsampled NGRIP ice core sulfate covers such a transitional period (Cooper et al., 2021) yet no evidence of S-MIF bearing sulfate is found. While further tracer-based fingerprinting (e.g, $\Delta^{17}O$ of ice core (NO_3^-)) is warranted to better understand any potential influence of STT processes on this geochemical imprint, here accounting for (i- iii), we argue that there exists another possibility of a geographically varying UV-influx during the investigated phases of the LGE event (Mukhopadhyay et al., 2025), which would make it feasible for sulfate sourced from similar sources to exhibit discernible anomalous characteristic in different hemispheres.

4. Conclusion and Implications

Our study provides first direct evidence of the formation of a UV 'window' during the LGE event. Despite the possibility of dilution effects impacting the S-MIF signal, the bi-polar ice-core sulfate record alternatively supports the notion of a geographically varying influence of the UV window formed from magnetic field collapse. Data-based global paleomagnetic field models could provide novel insights into the formation of the geomagnetic excursion linked UV window. Quantities, such as field morphology at the core-mantle boundary or individual spherical harmonic degree power variations

need to be accounted with caution (Korte et al., 2019). Modeling works relying on these parameters suggest that the excursion process during the Laschamp was mainly governed by axial dipole decay and recovery, without a significant influence from the equatorial dipole or non-dipole fields (Korte et al., 2019; Leonhardt et al., 2009; Laj et al., 2006; Panovska et al., 2017). This results in an excursional field behavior seen globally, but 'non-uniformly' at the Earth's surface and is supportive of the notion that the ensuing magnitude of the ozone depletion was also non-uniform fields (Korte et al., 2019; Laj et al., 2006). Studies of the effects of cosmic radiation during paleo-magnetospheric polarity transitions reveal that, with a reduction in dipole moment strength, lower latitudes including the tropical zone become accessible to high fluxes of lower-energy particles, ushering in zones of impact for diverse magnetospheric configurations (Mukhopadhyay et al., 2025). In the period of the overlapping bi-polar ice-core record, the excursion was strongest in the Indian Ocean and the south Atlantic Ocean as well as the southern Oceanic regions yet in the proximity of Antarctica (Korte et al., 2019; Mukhopadhyay et al., 2025). While in the Northern hemisphere, the expanded auroral zones towards the equator suggest such impact zones for high energy cosmic rays were further way from Greenland (Mukhopadhyay et al., 2025). Therefore, it is possible that the effect of the UV window (detected ≈ 41.6 ka BP) strongly materialized in the Southern Hemisphere than in the Northern hemisphere during the investigated period of the LGE event. However, further research is warranted to better understand the globality of the UV window during the entirety of the LGE event.

We also note that the atmospheric modeling of the NO_x-ozone chemistry is at odds with this notion (Cooper et al., 2021; Suter et al., 2014). Atmospheric modelling studies have provided quantitative estimates for ozone depletion during such events (Cooper et al., 2021; Suter et al., 2014; Norval et al., 2007; Winkler et al., 2008). For instance, during the LGE event, such modeling works estimated only ~ 5 % ozone loss in the lower stratosphere over Antarctica with a similar increase in tropospheric ozone mixing ratios and the opposite for the Arctic region (Cooper et al., 2021). Such a scenario would impede S-MIF-generating UV-induced photochemical processes. Furthermore, a

relatively higher ozone loss over the Arctic than over Antarctica should have led to the detection of the UV window in the northern hemisphere with effect strongly materialized in the northern polar ice-cores which is not the case. As such, considering the 'non-uniform' evolution of the magnetic field could be valuable in accurately modeling the ozone depletion during such events. The morphological alterations experienced by Earth's magnetosphere and its auroral zones together with the geochemical imprint shown in this study support the argument for further research on the evolving geomagnetic shielding behavior during geomagnetic excursions to better understand the environmental, atmospheric and climatic effects during such events.

Acknowledgments

The authors thank Jean-Robert Petit, colleagues Volodya Lipenkov and the Russian Vostok site consortium for their field endeavours and for allowing access to the VK ice-core archive and repository. We also thank Jorgen Peder Steffensen, Dorthe Dahl-Jensen and Anders Svensson from NGRIP ice-core consortium at the Neils Bohr Institute of the University of Copenhagen for providing the relevant samples. S.D. and J.S. acknowledge support from Anders Svensson for identifying the relevant NGRIP ice-core depths of interest using age-transfer calculations. S.D. acknowledges support from Elsa Gautier, Patrick Ginot, and Gregory Teste with lab-based operations and ice-core handling. This study was supported by the Marie Skłodowska-Curie Action Grant number 1010180 (to S.D.; hosted by J.S. and G.P.) and CNRS-INSU Les Enveloppes Fluides et l'Environnement (LEFE) grant (to G.P). Sulfur isotopes were measured on the IRISS analytical platform CNRS-RéGEF network.

Author Contributions

Conceptualization: Joel Savarino, Guillaume Paris, Julien Charreau, Sanjeev Dasari **Methodology:** Guillaume Paris, Joel Savarino, Alexis Lamothe, Sanjeev Dasari **Project management:** Sanjeev Dasari, Joel Savarino **Visualization:** Sanjeev Dasari **Writing – original draft:** Sanjeev Dasari,

Guillaume Paris, Julien Charreau, Joel Savarino **Writing – review & editing:** Sanjeev Dasari, Guillaume Paris, Julien Charreau, Alexis Lamothe, Joel Savarino

Data Availability Statement

All data is included in the manuscript and/or supporting information.

Conflict of Interest

The authors declare no conflict of interest relevant to this study.

References

Alexander, B., Thiemens, M. H., Farquhar, J., Kaufman, A. J., Savarino, J., & Delmas, R. J. (2003). East Antarctic ice core sulfur isotope measurements over a complete glacial-interglacial cycle. *Journal of Geophysical Research: Atmospheres*, *108*(D24). https://doi.org/10.1029/2003JD003513

Au Yang, D., Cartigny, P., Desboeufs, K., & Widory, D. (2019). Seasonality in the Δ 33 S measured in urban aerosols highlights an additional oxidation pathway for atmospheric SO 2. *Atmospheric Chemistry and Physics*, *19*(6), 3779-3796. https://doi.org/10.5194/acp-19-3779-2019

Baroni, M., Thiemens, M. H., Delmas, R. J., & Savarino, J. (2007). Mass-independent sulfur isotopic compositions in stratospheric volcanic eruptions. *Science*, *315*(5808), 84-87. http://doi.org/10.1126/science.1131754

Baroni, M., Savarino, J., Cole-Dai, J., Rai, V. K., & Thiemens, M. H. (2008). Anomalous sulfur isotope compositions of volcanic sulfate over the last millennium in Antarctic ice cores. *Journal of Geophysical Research: Atmospheres*, *113*(D20). https://doi.org/10.1029/2008JD010185

Burke, A., Present, T. M., Paris, G., Rae, E. C., Sandilands, B. H., Gaillardet, J., et al., (2018). Sulfur isotopes in rivers: Insights into global weathering budgets, pyrite oxidation, and the modern sulfur cycle. *Earth and Planetary Science Letters*, *496*, 168-177. https://doi.org/10.1016/j.epsl.2018.05.022

Burke, A., Moore, K. A., Sigl, M., Nita, D. C., McConnell, J. R., & Adkins, J. F. (2019). Stratospheric eruptions from tropical and extra-tropical volcanoes constrained using high-resolution sulfur isotopes in ice cores. *Earth and planetary science letters*, *521*, 113-119. http://doi.org/10.1016/j.epsl.2019.06.006

Bouchet, M., Landais, A., Grisart, A., Parrenin, F., Prié, F., Jacob, R., et al., (2023). The Antarctic Ice Core Chronology 2023 (AICC2023) chronological framework and associated timescale for the European Project for Ice Coring in Antarctica (EPICA) Dome C ice core. *Climate of the Past*, *19*(11), 2257-2286. https://doi.org/10.5194/cp-19-2257-2023

Channell, J. E. T., & Vigliotti, L. (2019). The role of geomagnetic field intensity in late quaternary evolution of humans and large mammals. *Reviews of Geophysics*, *57*(3), 709-738. https://doi.org/10.1029/2018RG000629

Cooper, A., Turney, C. S., Palmer, J., Hogg, A., McGlone, M., Wilmshurst, J., et al., (2021). A global environmental crisis 42,000 years ago. *Science*, *371*(6531), 811-818. http://doi.org/10.1126/science.abb8677

595 Cole-Dai, J., Ferris, D. G., Kennedy, J. A., Sigl, M., McConnell, J. R., Fudge, T. J et al., (2021).
596 Comprehensive record of volcanic eruptions in the Holocene (11,000 years) from the WAIS Divide,
597 Antarctica ice core. *Journal of geophysical research: Atmospheres*, *126*(7), e2020JD032855.
598 https://doi.org/10.1029/2020JD032855
599
600 Colman, J. J., Xu, X., Thiemens, M. H., & Trogler, W. C. (1996). Photopolymerization and mass-
601 independent sulfur isotope fractionations in carbon disulfide. *Science*, *273*(5276), 774-776.
602 http://doi.org/10.1126/science.273.5276.774
603
604 Dasari, S., Andersson, A., Stohl, A., Evangeliou, N., Bikkina, S., Holmstrand, H., et al., (2020).
605 Source quantification of South Asian black carbon aerosols with isotopes and
606 modeling. *Environmental science & technology*, *54*(19), 11771-11779.
607 https://doi.org/10.1021/acs.est.0c02193
608
609 Dasari, S., Andersson, A., Popa, M. E., Rockmann, T., Holmstrand, H., Budhavant, K., & Gustafsson,
610 O. (2021). Observational evidence of large contribution from primary sources for carbon monoxide in
611 the South Asian outflow. *Environmental science & technology*, *56*(1), 165-174.
612 https://doi.org/10.1021/acs.est.1c05486
613
614 Dasari, S., Paris, G., Charreau, J., & Savarino, J. (2022a). Sulfur-isotope anomalies recorded in
615 Antarctic ice cores as a potential proxy for tracing past ozone layer depletion events. *PNAS*
616 *nexus*, *1*(4), pgac170. https://doi.org/10.1093/pnasnexus/pgac170
617
618 Dasari, S., Paris, G., Saar, B., Pei, Q., Cong, Z., & Widory, D. (2022b). Sulfur isotope anomalies
619 (Δ33S) in urban air pollution linked to mineral-dust-associated sulfate. *Environmental Science &*
620 *Technology Letters*, *9*(7), 604-610. https://doi.org/10.1021/acs.estlett.2c00312

Dasari, S., Paris, G., Pei, Q., Cong, Z., & Widory, D. (2023). Tracing the origin of elevated springtime atmospheric sulfate on the southern Himalayan-Tibetan plateau. *Environmental Science: Advances*, *2*(8), 1110-1118. http://doi.org/10.1039/D3VA00085K

Dasari, S., & Widory, D. (2024). Retrospective isotopic analysis of summertime urban atmospheric sulfate in South Asia using improved source constraints. *ACS ES&T Air*, *1*(5), 357-364. https://doi.org/10.1021/acsestair.3c00060

Farquhar, J., Bao, H., & Thiemens, M. (2000). Atmospheric influence of Earth's earliest sulfur cycle. *Science*, *289*(5480), 756-758. http://doi.org/10.1126/science.289.5480.756

Gautier, E., Savarino, J., Erbland, J., Lanciki, A., & Possenti, P. (2016). Variability of sulfate signal in ice core records based on five replicate cores. *Climate of the Past*, *12*(1), 103-113. https://doi.org/10.5194/cp-12-103-2016

Gautier, E., Savarino, J., Erbland, J., & Farquhar, J. (2018). SO2 oxidation kinetics leave a consistent isotopic imprint on volcanic ice core sulfate. *Journal of Geophysical Research: Atmospheres*, *123*(17), 9801-9812. https://doi.org/10.1029/2018JD028456

Gautier, E., Savarino, J., Hoek, J., Erbland, J., Caillon, N., Hattori, S., et al., (2019). 2600-years of stratospheric volcanism through sulfate isotopes. *Nature communications*, *10*(1), 466. https://doi.org/10.1038/s41467-019-08357-0

Geng, L., Murray, L. T., Mickley, L. J., Lin, P., Fu, Q., Schauer, A. J., et al., (2017). Isotopic evidence of multiple controls on atmospheric oxidants over climate transitions. *Nature*, 546(7656), 133-136. https://doi.org/10.1038/nature22340

Geng, L., Savarino, J., Caillon, N., Gautier, E., Farquhar, J., Dottin Iii, J. W., et al., (2019). Intercomparison measurements of two 33 S-enriched sulfur isotope standards. *Journal of Analytical Atomic Spectrometry*, *34*(6), 1263-1271. http://doi.org/10.1039/C8JA00451J

Han, X., Guo, Q., Strauss, H., Liu, C., Hu, J., Guo, Z., et al., (2017). Multiple sulfur isotope constraints on sources and formation processes of sulfate in Beijing PM2. 5 aerosol. *Environmental science & technology*, *51*(14), 7794-7803. https://doi.org/10.1021/acs.est.7b00280

Hawks , J (2021). Comment on "A global environmental crisis 42,000 years ago". *Science*, *374*(6570), p.eabi8330. http://doi.org/10.1126/science.abh1878

Hattori, S., Schmidt, J. A., Johnson, M. S., Danielache, S. O., Yamada, A., Ueno, Y., & Yoshida, N. (2013). SO2 photoexcitation mechanism links mass-independent sulfur isotopic fractionation in cryospheric sulfate to climate impacting volcanism. *Proceedings of the National Academy of Sciences*, *110*(44), 17656-17661. https://doi.org/10.1073/pnas.1213153110

Herndon, J. M. (2020). Causes and consequences of geomagnetic field collapse. *J Geog Environ Earth Sci Intn*, *24*(9), 60-76. http://doi.org/10.9734/JGEESI/2020/v24i930256

Hodgson, D. A., Vyverman, W., Verleyen, E., Leavitt, P. R., Sabbe, K., Squier, A. H., & Keely, B. J. (2005). Late Pleistocene record of elevated UV radiation in an Antarctic lake. *Earth and Planetary Science Letters*, *236*(3-4), 765-772. https://doi.org/10.1016/j.epsl.2005.05.023

Hulston, J. R., & Thode, H. G. (1965). Variations in the S33, S34, and S36 contents of meteorites and their relation to chemical and nuclear effects. *Journal of Geophysical Research*, *70*(14), 3475-3484. https://doi.org/10.1029/JZ070i014p03475

Ishino, S., Hattori, S., Savarino, J., Legrand, M., Albalat, E., Albarede, F., et al., (2019). Homogeneous sulfur isotope signature in East Antarctica and implication for sulfur source shifts through the last glacial-interglacial cycle. *Scientific Reports*, *9*(1), 12378. https://doi.org/10.1038/s41598-019-48801-1

Jackson, A., Jonkers, A. R., & Walker, M. R. (2000). Four centuries of geomagnetic secular variation from historical records. *Philosophical Transactions of the Royal Society of London. Series A: Mathematical, Physical and Engineering Sciences*, *358*(1768), 957-990. https://doi.org/10.1098/rsta.2000.0569

Jourdain, B., & Legrand, M. (2002). Year-round records of bulk and size-segregated aerosol composition and HCl and HNO3 levels in the Dumont d'Urville (coastal Antarctica) atmosphere: Implications for sea-salt aerosol fractionation in the winter and summer. *Journal of Geophysical Research: Atmospheres*, *107*(D22), ACH-20. https://doi.org/10.1029/2002JD002471

Jongebloed, U. A., Schauer, A. J., Cole-Dai, J., Larrick, C. G., Wood, R., Fischer, T. P., et al., (2023). Underestimated passive volcanic sulfur degassing implies overestimated anthropogenic aerosol forcing. *Geophysical Research Letters*, *50*(1), e2022GL102061. https://doi.org/10.1029/2022GL102061

Jongebloed, U. A., Schauer, A. J., Hattori, S., Cole-Dai, J., Larrick, C. G., Salimi, S., et al., (2023). Sulfur isotopes quantify the impact of anthropogenic activities on industrial-era Arctic sulfate in a Greenland ice core. *Environmental Research Letters*, *18*(7), 074020. http://doi.org/10.1088/1748-9326/acdc3d

Kiyosu, Y. (1985). Isotopic composition of acid sulfate-chloride waters and volcanic steam from some volcanoes in northeastern Japan. *Journal of volcanology and geothermal research*, *26*(1-2), 25-36. https://doi.org/10.1016/0377-0273(85)90045-9

Korte, M., Brown, M. C., Panovska, S., & Wardinski, I. (2019). Robust characteristics of the Laschamp and Mono Lake geomagnetic excursions: Results from global field models. *Frontiers in Earth Science*, *7*, 86. https://doi.org/10.3389/feart.2019.00086

Laj, C., Kissel, C., & Roberts, A. P. (2006). Geomagnetic field behavior during the Iceland Basin and Laschamp geomagnetic excursions: A simple transitional field geometry?. *Geochemistry, Geophysics, Geosystems*, *7*(3). https://doi.org/10.1029/2005GC001122

Legrand, M., Preunkert, S., Wolff, E., Weller, R., Jourdain, B., & Wagenbach, D. (2017). Year-round records of bulk and size-segregated aerosol composition in central Antarctica (Concordia site)–Part 1: Fractionation of sea-salt particles. *Atmospheric Chemistry and Physics*, *17*(22), 14039-14054. https://doi.org/10.5194/acp-17-14039-2017

Leonard, K., Bell, R. E., Studinger, M., & Tremblay, L. B. (2004). Anomalous accumulation rates in the Vostok ice-core resulting from ice flow over Lake Vostok. http://doi.org/10.1029/2004GL021102

Leonhardt, R., Fabian, K., Winklhofer, M., Ferk, A., Laj, C., & Kissel, C. (2009). Geomagnetic field evolution during the Laschamp excursion. *Earth and Planetary Science Letters*, *278*(1-2), 87-95. https://doi.org/10.1016/j.epsl.2008.11.028

Lin, M., Zhang, X., Li, M., Xu, Y., Zhang, Z., Tao, J., ... & Thiemens, M. H. (2018). Five-S-isotope evidence of two distinct mass-independent sulfur isotope effects and implications for the modern and Archean atmospheres. *Proceedings of the National Academy of Sciences*, *115*(34), 8541-8546. https://doi.org/10.1073/pnas.1803420115

Lin, J., Svensson, A., Hvidberg, C. S., Lohmann, J., Kristiansen, S., Dahl-Jensen, D., et al., (2022). Magnitude, frequency and climate forcing of global volcanism during the last glacial period as seen in Greenland and Antarctic ice cores (60–9 ka). *Climate of the Past*, *18*(3), 485-506. https://doi.org/10.5194/cp-18-485-2022

Marshall, J. E., Lakin, J., Troth, I., & Wallace-Johnson, S. M. (2020). UV-B radiation was the Devonian-Carboniferous boundary terrestrial extinction kill mechanism. *Science Advances*, *6*(22), eaba0768. http://doi.org/10.1126/sciadv.aba0768

McConnell, J. R., Burke, A., Dunbar, N. W., Köhler, P., Thomas, J. L., Arienzo, M. M., et al., (2017). Synchronous volcanic eruptions and abrupt climate change∼ 17.7 ka plausibly linked by stratospheric ozone depletion. *Proceedings of the National Academy of Sciences*, *114*(38), 10035-10040. https://doi.org/10.1073/pnas.1705595114

Merrill, R. T., & McElhinny, M. W. (1983). *The Earth's magnetic field: Its history, origin and planetary perspective* (Vol. 401). London: Academic press.

Mukhopadhyay, A., Panovska, S., Garvey, R., Liemohn, M. W., Ganjushkina, N., Brenner, A., et al., (2025). Wandering of the auroral oval 41,000 years ago. *Science Advances*, *11*(16), eadq7275. http://doi.org/10.1126/sciadv.adq7275

Nielsen, L. T., Karlsson, N. B., & Hvidberg, C. S. (2015). Large-scale reconstruction of accumulation rates in northern Greenland from radar data. *Annals of Glaciology*, *56*(70), 70-78. http://doi.org/10.3189/2015AoG70A062

Norval, M., Cullen, A. P., De Gruijl, F. R., Longstreth, J., Takizawa, Y., Lucas, R. M., et al., (2007). The effects on human health from stratospheric ozone depletion and its interactions with climate change. *Photochemical & Photobiological Sciences*, *6*(3), 232-251. http://doi.org/10.1039/b700018a

Nowaczyk, N. R., Jiabo, L., Lamy, F., Lembke-Jene, L., & Arz, H. W. (2025). The Mono Lake and Laschamps geomagnetic excursions recorded by sediments in the Drake Passage. *Journal of Geophysical Research: Solid Earth*, *130*(1), e2024JB029835. https://doi.org/10.1029/2024JB029835

Ono, S. (2017). Photochemistry of sulfur dioxide and the origin of mass-independent isotope fractionation in Earth's atmosphere. *Annual Review of Earth and Planetary Sciences*, *45*, 301-329. https://doi.org/10.1146/annurev-earth-060115-012324

Panovska, S., & Constable, C. G. (2017). An activity index for geomagnetic paleosecular variation, excursions, and reversals. *Geochemistry, Geophysics, Geosystems*, *18*(4), 1366-1375. https://doi.org/10.1002/2016GC006668

Paris, G., Sessions, A. L., Subhas, A. V., & Adkins, J. F. (2013). MC-ICP-MS measurement of δ34S andΔ 33S in small amounts of dissolved sulfate. *Chemical Geology*, *345*, 50-61. https://doi.org/10.1016/j.chemgeo.2013.02.022

Paris, G. (2024). Determination of unbiased δ34S and Δ33S values by MC-ICP-MS using down to 30 nmol of sulfur. *Geostandards and Geoanalytical Research*, *48*(1), 29-42. https://doi.org/10.1111/ggr.12535

Paris, G., Adkins, J. F., Sessions, A. L., Webb, S. M., & Fischer, W. W. (2014). Neoarchean carbonate–associated sulfate records positive Δ33S anomalies. *Science*, *346*(6210), 739-741. http://doi.org/10.1126/science.1258211

Pearson, C., Sigl, M., Burke, A., Davies, S., Kurbatov, A., Severi, M., ... & Helmick, M. (2022). Geochemical ice-core constraints on the timing and climatic impact of Aniakchak II (1628 BCE) and Thera (Minoan) volcanic eruptions. *PNAS nexus*, *1*(2), pgac048. https://doi.org/10.1093/pnasnexus/pgac048

Pei, Q., Widory, D., Paris, G., Kang, S., Wan, X., Dasari, S., et al., (2026). Wildfires Drive Sulfur Isotope Anomalies on the Himalayan-Tibetan Plateau. *ACS ES&T Air*. https://doi.org/10.1021/acsestair.5c00493

Picin, A., Benazzi, S., Blasco, R., Hajdinjak, M., Helgen, K. M., Hublin, J. J., et al., (2021). Comment on “A global environmental crisis 42,000 years ago”. *Science*, *374*(6570), eabi8330. http://doi.org/10.1126/science.abi8330

Raisbeck, G. M., Yiou, F., Bourlès, D., Lorius, C., Jouzel, J., & Barkov, N. I. (1987). Evidence for two intervals of enhanced 10Be deposition in Antarctic ice during the last glacial period. *Nature*, *326*(6110), 273-277. https://doi.org/10.1038/326273a0

Raisbeck, G. M., Yiou, F., Jouzel, J., & Stocker, T. F. (2007). Direct north-south synchronization of abrupt climate change record in ice cores using Beryllium 10. *Climate of the Past*, *3*(3), 541-547. https://doi.org/10.5194/cp-3-541-2007

Raisbeck, G. M., Cauquoin, A., Jouzel, J., Landais, A., Petit, J. R., Lipenkov, V. Y., et al., (2017). An improved north–south synchronization of ice core records around the 41 kyr 10 Be peak. *Climate of the Past*, *13*(3), 217-229. https://doi.org/10.5194/cp-13-217-2017

Savarino, J., Romero, A., Cole-Dai, J., Bekki, S., & Thiemens, M. H. (2003). UV induced mass-independent sulfur isotope fractionation in stratospheric volcanic sulfate. *Geophysical Research Letters*, *30*(21). https://doi.org/10.1029/2003GL018134

Shaheen, R., Abaunza, M. M., Jackson, T. L., McCabe, J., Savarino, J., & Thiemens, M. H. (2014). Large sulfur-isotope anomaly in nonvolcanic sulfate aerosol and its implications for the Archean atmosphere. *Proceedings of the National Academy of Sciences*, *111*(33), 11979-11983. https://doi.org/10.1073/pnas.1406315111

Shen, Y., Zhang, Q., Xu, Y., Li, M., & Thiemens, M. H. (2024). Sulfur isotope anomalies in coal combustion: applications to the present and early Earth environments. *Proceedings of the National Academy of Sciences*, *121*(51), e2408199121. https://doi.org/10.1073/pnas.2408199121

Simon, Q., Thouveny, N., Bourlès, D. L., Valet, J. P., Bassinot, F., Ménabréaz, L., et al., (2016). Authigenic 10Be/9Be ratio signatures of the cosmogenic nuclide production linked to geomagnetic dipole moment variation since the Brunhes/Matuyama boundary. *Journal of Geophysical Research: Solid Earth*, *121*(11), 7716-7741. https://doi.org/10.1002/2016JB013335

Sigl, M., McConnell, J. R., Layman, L., Maselli, O., McGwire, K., Pasteris, D., et al., (2013). A new bipolar ice core record of volcanism from WAIS Divide and NEEM and implications for climate forcing of the last 2000 years. *Journal of Geophysical Research: Atmospheres*, *118*(3), 1151-1169. https://doi.org/10.1029/2012JD018603

Solomon, S., Crutzen, P. J., & Roble, R. G. (1982). Photochemical coupling between the thermosphere and the lower atmosphere: 1. Odd nitrogen from 50 to 120 km. *Journal of Geophysical Research: Oceans*, *87*(C9), 7206-7220. https://doi.org/10.1029/JC087iC09p07206

Solomon, S. (1999). Stratospheric ozone depletion: A review of concepts and history. *Reviews of geophysics*, *37*(3), 275-316. https://doi.org/10.1029/1999RG900008

Suter, I., Zech, R., Anet, J. G., & Peter, T. (2014). Impact of geomagnetic excursions on atmospheric chemistry and dynamics. *Climate of the Past*, *10*(3), 1183-1194. https://doi.org/10.5194/cp-10-1183-2014

Svensson, A., Dahl-Jensen, D., Steffensen, J. P., Blunier, T., Rasmussen, S. O., Vinther, B. M., et al., (2020). Bipolar volcanic synchronization of abrupt climate change in Greenland and Antarctic ice cores during the last glacial period. *Climate of the Past*, *16*(4), 1565-1580. https://doi.org/10.5194/cp-16-1565-2020

Uemura, R., Masaka, K., Iizuka, Y., Hirabayashi, M., Matsui, H., Matsumoto, R., et al., (2022). Soluble salts in deserts as a source of sulfate aerosols in an Antarctic ice core during the last glacial period. *Earth and Planetary Science Letters*, *578*, 117299. https://doi.org/10.1016/j.epsl.2021.117299

Usoskin, I. G., & Kovaltsov, G. A. (2008). Cosmic rays and climate of the Earth: Possible connection. *Comptes Rendus Geoscience*, *340*(7), 441-450. https://doi.org/10.1016/j.crte.2007.11.001

Valet, J. P., Savranskaia, T., Egli, R., Simon, Q., Bassinot, F., & Thouveny, N. (2024). Beryllium ten production and relative paleointensity for the past 1.2 million years. *Quaternary Science Reviews*, *344*, 108993. https://doi.org/10.1016/j.quascirev.2024.108993

Valet, J. P., & Valladas, H. (2010). The Laschamp-Mono lake geomagnetic events and the extinction of Neanderthal: a causal link or a coincidence?. *Quaternary Science Reviews*, *29*(27-28), 3887-3893. https://doi.org/10.1016/j.quascirev.2010.09.010

Whitehill, A. R., Jiang, B., Guo, H., & Ono, S. (2015). SO 2 photolysis as a source for sulfur mass-independent isotope signatures in stratospehric aerosols. *Atmospheric Chemistry and Physics*, *15*(4), 1843-1864. https://doi.org/10.5194/acp-15-1843-2015

Winkler, H., Sinnhuber, M., Notholt, J., Kallenrode, M. B., Steinhilber, F., Vogt, J., et al., (2008). Modeling impacts of geomagnetic field variations on middle atmospheric ozone responses to solar proton events on long timescales. *Journal of Geophysical Research: Atmospheres*, *113*(D2). https://doi.org/10.1029/2007JD008574

Yiou, F., Raisbeck, G. M., Baumgartner, S., Beer, J., Hammer, C., Johnsen, S., et al., (1997). Beryllium 10 in the Greenland ice core project ice core at summit, Greenland. *Journal of Geophysical Research: Oceans*, *102*(C12), 26783-26794. https://doi.org/10.1029/97JC01265

References in Supporting Information

Veres D, Bazin L, Landais A, Toyé Mahamadou Kele H, Lemieux-Dudon B, Parrenin F, Martinerie P, Blayo E, Blunier T, Capron E, Chappellaz J. (2013). The Antarctic ice-core chronology (AICC2023): an optimized multi-parameter and multi-site dating approach for the last 120 thousand years. *Climate of the Past*. *9*(4), 1733-1748. https://doi.org/10.5194/cp-9-1733-2013

Bazin L, Landais A, Lemieux-Dudon B, Toyé Mahamadou Kele H, Veres D, Parrenin F, Martinerie P, Ritz C, Capron E, Lipenkov V, Loutre M F. (2013). An optimized multi-proxy, multi-site Antarctic ice and gas orbital chronology (AICC2023): 120–800 ka. *Climate of the Past*. *9*(4), 1715-1731. https://doi.org/10.5194/cp-9-1715-2013

Svensson, A., Dahl-Jensen, D., Steffensen, J. P., Blunier, T., Rasmussen, S. O., Vinther, B. M., et al., (2020). Bipolar volcanic synchronization of abrupt climate change in Greenland and Antarctic ice cores during the last glacial period. *Climate of the Past*, *16*(4), 1565-1580. https://doi.org/10.5194/cp-16-1565-2020

Supporting Information: Polar ice-cores unravel the formation of a UV window during magnetic field collapse ~ 42 ka BP

Sanjeev Dasari[1], Guillaume Paris[2], Julien Charreau[2], Alexis Lamothe[3#], Joel Savarino[3]

[1]Department of Earth Sciences, University of Oxford, Oxford, United Kingdom

[2]Université de Lorraine, CNRS, CRPG, Nancy, France

[3]Institut des Géosciences de l'Environnement, University Grenoble Alpes, CNRS, IRD, Grenoble INP, Grenoble, France

[#]Now at International Center for Isotope Effects Research, Nanjing University, Nanjing, China

Contents of this file

1. Tables S1 to S5

Introduction This document is used to provide additional tables to supplement specific details mentioned in the manuscript.

913 **Table S1. S-isotope values for ice-core sulfate samples from Antarctica (site: Vostok)**. The mean and
914 standard deviations of the ensemble of the measurements are shown. Sampling resolution was increased for
915 ice-core VK-611 and VK-612. This data is not corrected for contribution from sea salt. NA refers to data not
916 available. The AICC2023 age chronology is followed here.

Average Depth (m)	Average Age (AICC2023; BP)	$\delta^{34}S$ (‰)		$\Delta^{33}S$ (‰)		Sulfate Flux kg km^{-1}yr^{-1}
		Mean	s.d.	Mean	s.d.	
607.07±0.04	41295±4	14.54	0.02	0.05	0.02	2
607.19±0.04	41307±4	14.58	0.02	0.06	0.02	1
607.31±0.04	41319±4	12.72	0.08	0.03	0.04	1
607.43±0.04	41331±4	12.68	0.09	0.17	0.05	2
607.55±0.04	41343±4	15.06	0.05	0.00	0.02	2
607.66±0.03	41353±3	13.39	0.04	0.04	0.04	2
607.75±0.03	41362±3	12.41	0.12	0.17	0.02	4
607.84±0.03	41371±3	14.30	0.10	0.04	0.03	4
607.93±0.03	41379±3	13.59	0.15	0.00	0.04	3
609.07±0.04	41483±4	12.86	0.12	0.13	0.03	2
609.19±0.04	41498±4	15.22	0.03	0.04	0.02	3

609.31±0.04	41511±4	15.16	0.03	0.05	0.04	2
609.43±0.04	41526±4	13.91	0.06	0.08	0.03	2
609.54±0.03	41538±3	13.58	0.10	0.04	0.05	2
609.63±0.03	41549±2	13.34	0.07	0.00	0.04	1
609.73±0.04	41561±4	14.21	0.12	0.03	0.05	3
610.04	41570.00	14.15	0.14	0.05	0.04	3
610.09	41574.50	13.34	0.12	0.01	0.07	3
610.13	41579.00	12.11	0.08	-0.08	0.10	4
610.18	41583.50	9.48	0.05	0.04	0.06	4
610.22	41587.00	14.00	0.06	0.03	0.14	3
610.27	41591.50	13.16	0.07	-0.03	0.12	3
610.31	41596.00	14.45	0.04	-0.02	0.12	4
610.36	41600.50	15.42	0.06	0.09	0.10	3
610.40	41604.00	11.82	0.11	0.41	0.07	6
610.45	41608.50	15.29	0.06	0.01	0.14	3
610.49	41613.00	12.12	0.04	-0.03	0.17	3
610.54	41617.50	12.91	0.06	0.03	0.17	3
610.58	41621.00	13.59	0.11	0.17	0.10	3
610.63	41625.50	13.57	0.07	0.00	0.05	3
610.67	41630.00	10.66	0.04	0.25	0.13	3

610.72	41634.50	11.94	0.14	0.03	0.07	2
610.76	41638.00	13.27	0.02	-0.02	0.07	3
610.81	41642.50	14.45	0.10	0.02	0.12	3
610.85	41647.00	15.23	0.10	0.01	0.16	3
610.90	41651.50	13.43	0.05	0.01	0.06	3
610.94	41655.00	14.90	0.05	0.06	0.08	4
610.99	41659.50	14.38	0.03	0.03	0.06	3
611.07±0.03	41665±3	13.42	0.13	0.19	0.04	3
611.18±0.04	41678±4					
611.31±0.04	41690±4	14.15	0.04	0.04	0.01	3
611.43±0.03	41701±3	14.72	0.11	0.04	0.07	3
611.52±0.04	41711±3	11.50	0.05	0.00	0.06	3
611.63±0.04	41722±4	11.93	0.08	-0.02	0.06	3
611.77±0.04	41736±3	14.45	0.15	0.04	0.07	3
611.92±0.07	41749±3	14.62	0.09	0.06	0.06	5
612.09±0.04	41762±5	13.37	0.07	0.03	0.05	4
612.22±0.04	41774±5	14.94	0.08	0.10	0.06	3
612.36±0.04	41787±5	15.39	0.07	0.04	0.07	3
612.51±0.04	41802±5	15.23	0.10	0.03	0.06	2
612.65±0.03	41814±3	15.37	0.09	0.06	0.07	3

612.76±0.04	41825±5	11.40	0.10	0.04	0.03	4
612.87±0.04	41838±5	14.90	0.06	0.07	0.07	4
612.96±0.04	41850±6	9.40	0.13	0.03	0.09	4
613.13±0.04	41865±5	12.27	0.09	0.02	0.03	3
613.27±0.04	41882±5	11.53	0.09	0.13	0.05	4
613.38±0.03	41896±3					
613.49±0.04	41910±5	4.62	0.05	0.11	0.06	6
613.63±0.04	41926±5	10.14	0.08	0.07	0.05	3
613.74±0.03	41940±3	12.26	0.08	0.09	0.07	4
614.10±0.05	41957±5	10.84	0.15	0.18	0.08	4
614.27±0.06	41977±6	11.81	0.08	0.08	0.16	4
614.45±0.06	41997±5	4.51	0.09	0.07	0.07	4
614.62±0.06	42017±6	4.40	0.14	0.05	0.10	6
614.77±0.03	42034±3					
614.92±0.03	42048±3	4.61	0.15	0.02	0.14	12

Table S2. S-isotope values for ice-core sulfate samples from Greenland (site: NGRIP). The mean and standard deviations of the ensemble of the measurements are shown. This data is not corrected for contribution from sea salt. NA refers to data not available. The AICC2023 age chronology is followed here.

Average Depth (m)	Average Age (AICC2023; BP)	$\delta^{34}S$ (‰)		$\Delta^{33}S$ (‰)		Sulfate Flux kg km^{-1}yr^{-1}
		Mean	s.d.	Mean	s.d.	
2126.34±0.04	41521±3	6.75	0.12	0.04	0.06	48
2126.46±0.04	41529±3	7.23	0.13	-0.11	0.11	37
2126.58±0.04	41538±3	NA				
2126.70±0.04	41547±3	6.14	0.02	0.01	0.05	69
2126.82±0.04	41556±3	6.65	0.08	-0.03	0.10	68
2126.94±0.04	41565±3	6.46	0.11	0.00	0.05	36
2127.06±0.04	41574±3	NA				
2127.18±0.04	41583±3	7.00	0.03	-0.05	0.12	55
2127.30±0.04	41592±3	4.61	0.07	-0.08	0.07	54
2127.42±0.04	41601±3	6.27	0.06	0.02	0.05	78
2127.54±0.04	41619±3	6.75	0.14	-0.03	0.11	71
2127.66±0.04	41628±3	6.70	0.05	0.05	0.05	59
2127.78±0.04	41637±3	6.48	0.28	0.00	0.06	36
2127.90±0.04	41646±3	6.99	0.05	-0.05	0.05	45

2128.02±0.04	41655±3	7.12	0.07	0.00	0.04	57
2128.14±0.04	41664±3					
2128.26±0.04	41673±3	6.71	0.17	0.01	0.05	98
2128.38±0.04	41682±3	6.68	0.15	0.03	0.07	29
2128.50±0.04	41691±3	NA				
2128.62±0.04	41700±3	6.16	0.07	0.04	0.05	66
2128.74±0.04	41709±3	NA				
2129.00±0.05	41719±4	5.59	0.07	0.00	0.03	62

920

921 **Table S3. Age transfer function for identifying corresponding periods of the Laschamp geomagnetic**
922 **excursion on the NGRIP ice-cores**. The periods are corresponding to the periods where the maximum isotopic
923 anomalies were detected in the Vostok ice-cores. Bi-polar mp = bi-polar volcanic match point from Table 1
924 and Table S2 from Svensson et al. 2020. For the bi-polar matching we first convert AICC2023 ages (41503-
925 41680) to AICC2012 ages (Veres et al., 2013; Bazin et al., 2013).
926

Event	AICC2012age (BP 1950)	Vostok depth (m)	EDML depth (m)	NGRIP depth (m)	GICC05 age (b2k)
Bi-polar mp			1378.51	2123.98	
Interval start	41540	609.71	1382.10	**2126.52**	41623
Interval end	41710	611.53	1385.42	**2128.87**	41790
Bi-polar mp			1387.31	2130.21	

927 **Table S4. Bayesian statistical source apportionment results for VOSTOK ice core sulfate samples**.

$\delta^{34}S$ (‰)	Source	Source Fraction	SD	95% CI Lower	95% CI Upper	CV (%)
	Biogenic	0.78	0.04	0.65	0.84	6
14.54 ± 0.02	Volcanic	0.08	0.03	0.07	0.20	24
	Terrestrial	0.14	0.02	0.06	0.16	24
	Biogenic	0.81	0.04	0.65	0.84	6
14.58 ± 0.02	Volcanic	0.06	0.03	0.07	0.20	24
	Terrestrial	0.14	0.02	0.06	0.16	24
	Biogenic	0.58	0.05	0.61	0.80	7
12.72 ± 0.08	Volcanic	0.22	0.03	0.10	0.25	20
	Terrestrial	0.20	0.02	0.06	0.16	25
	Biogenic	0.71	0.05	0.61	0.80	7
12.68 ± 0.09	Volcanic	0.22	0.03	0.10	0.25	20
	Terrestrial	0.07	0.02	0.06	0.16	25
	Biogenic	0.86	0.04	0.66	0.85	6
15.06 ± 0.05	Volcanic	0.01	0.03	0.06	0.19	25
	Terrestrial	0.13	0.02	0.06	0.16	24
	Biogenic	0.74	0.04	0.63	0.82	6.7
13.39 ± 0.04	Volcanic	0.17	0.03	0.09	0.23	22
	Terrestrial	0.09	0.02	0.06	0.16	25
	Biogenic	0.72	0.05	0.60	0.8	7
12.41 ± 0.12	Volcanic	0.25	0.03	0.11	0.26	20
	Terrestrial	0.03	0.02	0.06	0.16	25
	Biogenic	0.85	0.04	0.65	0.84	6
14.30 ± 0.10	Volcanic	0.11	0.03	0.07	0.21	23
	Terrestrial	0.04	0.02	0.06	0.16	24

	Biogenic	0.79	0.04	0.63	0.83	6
13.59 ± 0.15	Volcanic	0.16	0.03	0.08	0.22	22
	Terrestrial	0.05	0.02	0.06	0.16	25
	Biogenic	0.65	0.05	0.61	0.81	7
12.86 ± 0.12	Volcanic	0.23	0.03	0.10	0.24	21
	Terrestrial	0.12	0.02	0.06	0.16	25
	Biogenic	0.88	0.04	0.67	0.85	6
15.22 ± 0.03	Volcanic	0.01	0.03	0.06	0.19	25
	Terrestrial	0.11	0.02	0.06	0.16	24
	Biogenic	0.82	0.04	0.67	0.85	6
15.16 ± 0.03	Volcanic	0.00	0.03	0.06	0.19	26
	Terrestrial	0.18	0.02	0.06	0.16	24
	Biogenic	0.75	0.04	0.64	0.83	6
13.91 ± 0.06	Volcanic	0.14	0.03	0.08	0.21	23
	Terrestrial	0.11	0.02	0.06	0.16	25
	Biogenic	0.74	0.04	0.63	0.83	6.7
13.58 ± 0.10	Volcanic	0.17	0.03	0.08	0.22	22
	Terrestrial	0.09	0.02	0.06	0.16	25
	Biogenic	0.67	0.04	0.63	0.82	6
13.34 ± 0.07	Volcanic	0.17	0.03	0.09	0.23	22
	Terrestrial	0.16	0.02	0.06	0.16	25
	Biogenic	0.86	0.04	0.65	0.83	6.5
14.21 ± 0.12	Volcanic	0.11	0.03	0.07	0.21	23
	Terrestrial	0.03	0.02	0.06	0.16	24
	Biogenic	0.84	0.04	0.64	0.83	6.5
14.15 ± 0.14	Volcanic	0.12	0.03	0.08	0.21	23

	Terrestrial	0.04	0.02	0.06	0.16	24
	Biogenic	0.76	0.04	0.63	0.82	6
13.34 ± 0.12	Volcanic	0.15	0.03	0.09	0.23	22
	Terrestrial	0.09	0.02	0.06	0.16	25
	Biogenic	0.70	0.05	0.59	0.79	7.3
12.11 ± 0.08	Volcanic	0.23	0.03	0.12	0.27	20
	Terrestrial	0.07	0.02	0.06	0.16	25
	Biogenic	0.52	0.05	0.51	0.72	8
9.48 ± 0.05	Volcanic	0.44	0.04	0.18	0.351	16
	Terrestrial	0.05	0.02	0.06	0.174	24
	Biogenic	0.83	0.04	0.64	0.83	6.7
14.00 ± 0.06	Volcanic	0.12	0.03	0.08	0.22	23
	Terrestrial	0.05	0.02	0.06	0.16	25
	Biogenic	0.76	0.04	0.62	0.81	6
13.16 ± 0.07	Volcanic	0.18	0.03	0.09	0.23	21
	Terrestrial	0.05	0.02	0.06	0.16	25
	Biogenic	0.87	0.04	0.65	0.84	6
14.45 ± 0.04	Volcanic	0.09	0.03	0.07	0.20	24
	Terrestrial	0.04	0.02	0.06	0.16	24
	Biogenic	0.92	0.04	0.67	0.85	6
15.42 ± 0.06	Volcanic	0.01	0.03	0.06	0.18	26
	Terrestrial	0.07	0.02	0.06	0.16	24
	Biogenic	0.69	0.05	0.58	0.78	7
11.82 ± 0.11	Volcanic	0.29	0.03	0.12	0.28	19
	Terrestrial	0.02	0.02	0.06	0.16	25
15.29 ± 0.06	Biogenic	0.92	0.04	0.67	0.85	6

	Volcanic	0.01	0.03	0.06	0.18	25
	Terrestrial	0.07	0.02	0.06	0.16	24
	Biogenic	0.69	0.05	0.59	0.79	7
12.12 ± 0.04	Volcanic	0.26	0.03	0.12	0.27	20
	Terrestrial	0.05	0.02	0.06	0.16	25
	Biogenic	0.75	0.05	0.61	0.81	7
12.91 ± 0.06	Volcanic	0.20	0.03	0.10	0.24	21
	Terrestrial	0.04	0.02	0.06	0.16	25
	Biogenic	0.80	0.04	0.63	0.83	6
13.59 ± 0.11	Volcanic	0.15	0.03	0.08	0.22	22
	Terrestrial	0.05	0.02	0.06	0.16	25
	Biogenic	0.79	0.04	0.63	0.82	6
13.57 ± 0.07	Volcanic	0.16	0.03	0.08	0.22	22
	Terrestrial	0.05	0.02	0.06	0.16	25
	Biogenic	0.58	0.05	0.55	0.75	7
10.66 ± 0.04	Volcanic	0.37	0.04	0.15	0.31	17
	Terrestrial	0.05	0.02	0.06	0.17	25
	Biogenic	0.67	0.05	0.58	0.78	7.4
11.94 ± 0.14	Volcanic	0.27	0.03	0.12	0.27	19
	Terrestrial	0.06	0.02	0.06	0.16	25
	Biogenic	0.76	0.04	0.62	0.82	6.8
13.27 ± 0.02	Volcanic	0.19	0.03	0.09	0.23	22
	Terrestrial	0.05	0.02	0.06	0.16	25
	Biogenic	0.87	0.04	0.65	0.84	6.4
14.45 ± 0.10	Volcanic	0.09	0.03	0.07	0.20	24
	Terrestrial	0.04	0.02	0.06	0.16	24
15.23 ± 0.10	Biogenic	0.93	0.04	0.67	0.85	6

	Volcanic	0.03	0.03	0.06	0.19	25
	Terrestrial	0.04	0.02	0.06	0.16	24
	Biogenic	0.77	0.04	0.63	0.82	6
13.43 ± 0.05	Volcanic	0.18	0.03	0.09	0.22	22
	Terrestrial	0.05	0.02	0.06	0.16	25
	Biogenic	0.89	0.04	0.66	0.84	6
14.90 ± 0.05	Volcanic	0.06	0.03	0.07	0.20	24
	Terrestrial	0.04	0.02	0.06	0.16	24
	Biogenic	0.42	0.04	0.65	0.84	6.4
14.38 ± 0.03	Volcanic	0.52	0.03	0.07	0.21	23
	Terrestrial	0.06	0.02	0.06	0.16	24
	Biogenic	0.78	0.04	0.63	0.82	6.7
13.42 ± 0.13	Volcanic	0.17	0.03	0.09	0.22	22
	Terrestrial	0.05	0.02	0.06	0.16	25
	Biogenic	0.84	0.04	0.64	0.83	6.5
14.15 ± 0.04	Volcanic	0.13	0.03	0.08	0.21	23
	Terrestrial	0.03	0.02	0.06	0.16	24
	Biogenic	0.88	0.04	0.66	0.84	6
14.72 ± 0.11	Volcanic	0.07	0.03	0.07	0.20	23
	Terrestrial	0.05	0.02	0.06	0.16	24
	Biogenic	0.64	0.05	0.57	0.77	7
11.50 ± 0.05	Volcanic	0.33	0.04	0.13	0.29	19
	Terrestrial	0.04	0.02	0.06	0.16	25
	Biogenic	0.69	0.05	0.58	0.78	7
11.93 ± 0.08	Volcanic	0.26	0.03	0.12	0.27	19
	Terrestrial	0.05	0.02	0.06	0.16	25

	Biogenic	0.86	0.04	0.65	0.84	6
14.45 ± 0.15	Volcanic	0.09	0.03	0.07	0.20	24
	Terrestrial	0.05	0.02	0.06	0.16	24
	Biogenic	0.88	0.04	0.65	0.84	6
14.62 ± 0.09	Volcanic	0.08	0.03	0.07	0.20	24
	Terrestrial	0.04	0.02	0.06	0.16	24
	Biogenic	0.78	0.04	0.63	0.82	6
13.37 ± 0.07	Volcanic	0.18	0.03	0.09	0.23	22
	Terrestrial	0.04	0.02	0.06	0.16	25
	Biogenic	0.91	0.04	0.66	0.84	6
14.94 ± 0.08	Volcanic	0.03	0.03	0.07	0.20	24
	Terrestrial	0.06	0.02	0.06	0.16	24
	Biogenic	0.92	0.04	0.67	0.85	6
15.39 ± 0.07	Volcanic	0.01	0.03	0.06	0.18	26
	Terrestrial	0.07	0.02	0.06	0.16	24
	Biogenic	0.91	0.04	0.67	0.85	6
15.23 ± 0.10	Volcanic	0.03	0.03	0.06	0.19	25
	Terrestrial	0.07	0.02	0.06	0.16	24
	Biogenic	0.93	0.04	0.67	0.85	6
15.37 ± 0.09	Volcanic	0.01	0.03	0.06	0.18	26
	Terrestrial	0.06	0.02	0.06	0.16	24
	Biogenic	0.63	0.05	0.57	0.77	7.6
11.40 ± 0.10	Volcanic	0.33	0.04	0.13	0.29	18
	Terrestrial	0.04	0.02	0.06	0.16	25
	Biogenic	0.89	0.04	0.66	0.84	6
14.90 ± 0.06	Volcanic	0.07	0.03	0.07	0.20	24

	Terrestrial	0.04	0.02	0.06	0.16	24
	Biogenic	0.49	0.05	0.51	0.71	8
9.40 ± 0.13	Volcanic	0.46	0.04	0.18	0.35	16
	Terrestrial	0.04	0.02	0.06	0.17	24
	Biogenic	0.68	0.05	0.60	0.79	7
12.27 ± 0.09	Volcanic	0.26	0.03	0.11	0.26	20
	Terrestrial	0.06	0.02	0.06	0.16	25
	Biogenic	0.63	0.05	0.57	0.77	7
11.53 ± 0.09	Volcanic	0.27	0.04	0.13	0.29	19
	Terrestrial	0.10	0.02	0.06	0.16	25
	Biogenic	0.17	0.05	0.38	0.58	10
4.62 ± 0.05	Volcanic	0.78	0.04	0.32	0.50	11
	Terrestrial	0.78	0.02	0.05	0.15	24
	Biogenic	0.55	0.05	0.53	0.74	8
10.14 ± 0.08	Volcanic	0.40	0.04	0.16	0.32	17
	Terrestrial	0.05	0.02	0.06	0.17	25
	Biogenic	0.70	0.05	0.60	0.79	7
12.26 ± 0.08	Volcanic	0.26	0.03	0.11	0.26	20
	Terrestrial	0.03	0.02	0.06	0.16	25
	Biogenic	0.61	0.05	0.55	0.76	7
10.84 ± 0.15	Volcanic	0.36	0.04	0.14	0.30	18
	Terrestrial	0.04	0.02	0.06	0.17	25
	Biogenic	0.67	0.05	0.58	0.78	7
11.81 ± 0.08	Volcanic	0.29	0.03	0.12	0.28	19
	Terrestrial	0.03	0.02	0.06	0.16	25
4.51 ± 0.09	Biogenic	0.15	0.05	0.38	0.57	10

	Volcanic	0.80	0.04	0.32	0.50	11
	Terrestrial	0.06	0.02	0.05	0.15	24
	Biogenic	0.17	0.05	0.37	0.57	10
4.40 ± 0.14	Volcanic	0.80	0.04	0.33	0.51	11
	Terrestrial	0.03	0.02	0.05	0.15	24
	Biogenic	0.18	0.05	0.38	0.58	10
4.61 ± 0.15	Volcanic	0.81	0.04	0.32	0.50	11
	Terrestrial	0.01	0.02	0.05	0.15	24

946 **Table S5. Bayesian statistical source apportionment results for NGRIP ice core sulfate samples**.

947

$\delta^{34}S$ (‰)	Source	Source Fraction	SD	95% CI Lower	95% CI Upper	CV (%)
	Biogenic	0.08	0.02	0.03	0.14	31
6.75 ± 0.12	Volcanic	0.67	0.05	0.56	0.77	7
	Terrestrial	0.24	0.04	0.17	0.33	17
	Biogenic	0.09	0.02	0.04	0.15	31
7.23 ± 0.13	Volcanic	0.62	0.05	0.52	0.72	8
	Terrestrial	0.28	0.04	0.20	0.38	15
	Biogenic	0.07	0.02	0.03	0.12	33
6.14 ± 0.02	Volcanic	0.71	0.04	0.61	0.80	6
	Terrestrial	0.21	0.03	0.14	0.30	17
	Biogenic	0.07	0.02	0.03	0.13	32
6.65 ± 0.08	Volcanic	0.68	0.05	0.57	0.77	7
	Terrestrial	0.24	0.04	0.16	0.33	16
	Biogenic	0.07	0.02	0.03	0.13	32
6.46 ± 0.11	Volcanic	0.69	0.04	0.59	0.79	7
	Terrestrial	0.23	0.04	0.15	0.31	17
	Biogenic	0.08	0.02	0.04	0.15	31
7.00 ± 0.03	Volcanic	0.64	0.05	0.54	0.74	8
	Terrestrial	0.26	0.04	0.19	0.36	16
	Biogenic	0.04	0.01	0.01	0.08	39
4.61 ± 0.07	Volcanic	0.87	0.03	0.79	0.92	3
	Terrestrial	0.08	0.02	0.05	0.13	23
	Biogenic	0.07	0.02	0.03	0.13	32
6.27 ± 0.06	Volcanic	0.70	0.04	0.60	0.79	6

	Terrestrial	0.22	0.03	0.15	0.31	17
	Biogenic	0.08	0.02	0.03	0.14	32
6.75 ± 0.14	Volcanic	0.67	0.05	0.56	0.77	7
	Terrestrial	0.24	0.04	0.17	0.33	17
	Biogenic	0.07	0.02	0.03	0.14	31
6.70 ± 0.05	Volcanic	0.67	0.05	0.57	0.77	7
	Terrestrial	0.24	0.04	0.16	0.33	16
	Biogenic	0.07	0.02	0.03	0.13	33
6.48 ± 0.28	Volcanic	0.69	0.05	0.58	0.78	7
	Terrestrial	0.23	0.04	0.15	0.31	17
	Biogenic	0.08	0.02	0.04	0.15	31
6.99 ± 0.05	Volcanic	0.64	0.05	0.54	0.74	8
	Terrestrial	0.26	0.04	0.19	0.36	16
	Biogenic	0.08	0.02	0.04	0.15	30
7.12 ± 0.07	Volcanic	0.63	0.05	0.52	0.73	8
	Terrestrial	0.27	0.04	0.20	0.37	16
	Biogenic	0.07	0.02	0.03	0.14	32
6.71 ± 0.17	Volcanic	0.67	0.05	0.56	0.77	7
	Terrestrial	0.24	0.04	0.16	0.33	17
	Biogenic	0.07	0.02	0.03	0.14	31
6.68 ± 0.15	Volcanic	0.67	0.05	0.57	0.77	7
	Terrestrial	0.24	0.04	0.16	0.33	17
	Biogenic	0.07	0.02	0.03	0.12	33
6.16 ± 0.07	Volcanic	0.71	0.04	0.60	0.80	6
	Terrestrial	0.21	0.03	0.14	0.30	17
	Biogenic	0.05	0.02	0.02	0.10	34
5.59 ± 0.07	Volcanic	0.78	0.04	0.69	0.85	5

	Terrestrial	0.16	0.02	0.10	0.21	17

948